Universidad Zaragoza
1542

Trabajo Fin de Máster

Effects of Missing Data on Heart Rate Variability Metrics

Efectos de la Pérdida de Datos en las Métricas de Variabilidad de Ritmo Cardíaco

Autor

Diego Cajal Orleans

Directora

Raquel Bailón Luesma

Codirector

David Hernando Jumilla

Escuela de Ingeniería y Arquitectura

2020

RESUMEN

La explosión en el mercado de dispositivos *wearables* ha supuesto una revolución en el ámbito de la monitorización de la salud. Gran parte de la población, incluida la población no paciente, posee dispositivos de pulsera capaces de detectar sus latidos a lo largo de todo el día. Junto con las ventajas que esto supone, aparecen nuevos retos. Uno de ellos es la estabilidad de la calidad de la señal. Los movimientos constantes de estos dispositivos hacen que se produzcan grandes pérdidas de datos, que pueden ocasionar un deterioro de las mediciones. Esto es especialmente relevante en los dispositivos que analizan la variabilidad de ritmo cardíaco, una técnica que permite inferir información del sistema nervioso autónomo de forma no invasiva a partir del control que éste ejerce sobre el sistema circulatorio. Esta técnica necesita que todos los pulsos sean detectados para funcionar correctamente, por lo que la pérdida de datos supone inevitablemente un deterioro. Este trabajo se centra en investigar cómo se produce esta degradación para diferentes métodos y qué técnicas se pueden utilizar para reducirla. Para ello, se ha desarrollado un método de simulación de pérdida de pulsos que permite analizar los dos tipos de errores que se suelen dar: errores aleatoriamente distribuidos y en ráfagas. A su vez, se propone un nuevo método de rellenado de pulsos como una posibilidad de preprocesado, que obtiene mejores resultados que el método de referencia. Dependiendo de la aplicación y de los requerimientos de los dispositivos, se sugieren los métodos más robustos teniendo en cuenta también su coste y la información que proveen. Los métodos se han probado en una base de datos con 17 sujetos sometidos a una prueba de mesa basculante, que permite provocar cambios en la activación del sistema nervioso autónomo sin involucrar al sistema central o causar actividad en los músculos. Las métricas se han comparado tanto en la degradación de sus valores como en la capacidad para distinguir los cambios provocados por la prueba de mesa basculante.

ABSTRACT

The boom in the wearable device market has led to a revolution in the field of health monitoring. A large part of the population, including the non-patient population, has wrist devices capable of detecting their heartbeats throughout the day. Along with the advantages this brings, new challenges are emerging. One of them is the stability of the signal quality. The constant movements of these devices cause large data losses, which can lead to a deterioration of the measurements. This is especially relevant in devices that analyze heart rate variability, a technique that allows autonomous nervous system information to be inferred in a non-invasive way from the control it exerts over the circulatory system. This technique requires all pulses to be detected in order to work properly, so loss of data inevitably leads to deterioration. This work focuses on investigating how this degradation occurs for different methods and which techniques can be used to reduce it. For this purpose, a method of pulse loss simulation has been developed to analyze the two types of errors that usually arise: randomly distributed errors and bursts. At the same time, a new method for filling in pulses is proposed as a preprocessing option, which obtains better results than the reference method. Depending on the application and the requirements of the devices, the most robust methods are suggested taking into account also their cost and the information they provide. The methods have been tested in a database with 17 subjects undergoing a tilt-table test, which allows for changes in the activation of the autonomic nervous system without involving the central system or causing activity in the muscles. The metrics have been compared both in the degradation of their values and in the ability to distinguish the changes caused by the tilt-table test.

Contents

Chapter 1

Introduction

1.1 Context

This work has been realized within the Biomedical Signal Interpretation & Computational Simulation group of the University of Zaragoza and the Centro de Investigación Biomédica en Red - Bioingeniería, Biomateriales y Nanomedicina (CIBER-BBN). The objectives and scope of this project are part of a wider research on robust non-invasive ANS monitoring using wearable devices, within the context of the Biomedical Engineering PhD program at University of Zaragoza. The need for a research on the effects of missing data in Heart Rate Variability (HRV) metrics is motivated by a previous work using a wrist device: Cajal *et al.* Parasympathetic characterization guided by respiration from wrist peripheral venous pressure waveform. *Computing in Cardiology* 2020.

1.2 Motivation

For several decades, HRV has been a widely researched field because of its ability to evaluate Autonomic Nervous System (ANS) information in a non-invasive way [1]. This information became very important following the discovery that different cardiac pathologies, including sudden cardiac death, are related to ANS impairments [2]. The ANS is a control system that innervates internal organs and regulates body processes such as heart and respiratory rate, blood pressure, urination and digestion. Its action on the organs is conducted through two divisions: the sympathetic and the parasympathetic, each specialized in situations of stress (sympathetic) and rest (parasympathetic), and normally with opposite effects on the same organ. Although both sympathetic and parasympathetic act simultaneously, one can predominate over the other. For example, during a rest situation, the parasympathetic division slows the heart rate, decreases the blood pressure and stimulates digestion. On the other hand, during an acute stress situation (fight-or-flight response), there will be a withdrawal of the parasympathetic activity followed by a sympathetic activation,

which acts by increasing heart rate and blood pressure and slowing down less important body processes at that time such as digestion, besides other effects like pupils and airways dilation and sweat. Measuring the prevalence of one division over the other has become critical, as it has been demonstrated that an increase in sympathetic activity, or a reduction in vagal activity - the vagus nerve is the main parasympathetic control of the heart - is associated with cardiovascular diseases such as lethal arrhythmias [2]. The relative dominance of one ANS branch over the other is called sympathovagal balance.

As mentioned, HRV is a powerful tool for assessing the autonomic state, since both sympathetic and parasympathetic divisions act over the heart, controlling aspects such as Heart Rate (HR) and contractility. Heart rate is modulated by the Sinoatrial Node (SA node), located on the right atrium wall. This node is the natural pacemaker of the heart, the place where the heartbeats begin. The SA node is formed by cells with the capability to produce an electrical impulse, called action potential, which travels along the heart tissue, provoking the heart to contract. This action potential is triggered by the SA node cells themselves in a rhythmic way, maintaining a more or less constant rate. However, the innervation of the ANS over the SA node causes the action potentials to become more or less frequents, thus provoking the increasing or the decreasing of the heart rate. The sympathetic branch of the ANS causes an increase in HR, meanwhile the parasympathetic, via vagus nerve, has the opposite effect. The combined effect of both branches of the ANS modulates the HR over time trying to adjust it to the physiological needs of blood supply to the tissues.

Taking advantage of this neural modulation of the heart rate, there are many methods that can provide information about the ANS from HRV. Some are based on the time dependence of the beats, others on the frequency, and even on non-linear interrelationships or symbolic abstractions. A further explanation of the methods examined in this thesis can be found in Chapter 3.

HRV can be easily obtained by placing electrodes on the patient skin to obtain a signal proportional to the heart electrical activity. This well-known technique is called electrocardiography (ECG). Once the ECG signal is obtained, pulse detection is very straightforward (*e.g.*, Pan–Tompkins algorithm, wavelet methods, etc.). However, having a clean waveform to look for reference points is not always assured. Noise induced by the electronics, artifacts caused by movements, other noises like under skin muscles electrical activity, etc., can dramatically distort the signals until it becomes impossible to find any fiducial point in a beat period, downgrading the performance of the ANS assessment methods. This has taken on a major significance in the last decade with the massive use of wearables in health care applications. These devices allow for the monitoring of large volumes of subjects, whether they suffer from health disorders or not, in an uninterrupted manner without causing any discomfort to the bearer. Often camouflaged as watches with an elegant design, wrist devices dominate the market. However, such devices suffer from a very low

signal quality compared to clinic monitoring techniques such as ECG. In fact, they usually make use of photoplethysmography, a technique that measures changes in blood volume, rather than the electrical activity of the heart. It is considered that this signal is a good surrogate for the electrocardiographic signal to obtain HRV but also much more sensitive to artifacts [3].

Although the use of wearables is widespread worldwide, most devices do not allow HRV analysis but provide only the mean heart rate. The great advantage of the mean heart rate is that it is a very robust metric, not sensitive to large data losses suffered by wearables throughout the day due to constant movements of the wearer. On the other hand, the information that can be obtained from this metric is limited. Therefore, it is necessary to investigate and develop methods for HRV analysis which are robust to large data losses.

1.3 Objectives

This work has three objectives:

- The evaluation of different HRV methods to compare their degradation due to missing data, in order to obtain a general idea of its limitations.
- The proposal of a novel method to deal with missing data for robustness improvement in HRV analysis derived from wearable devices.
- The development of a missing data simulation protocol. Two different types of error distributions that may occur in the practical case will be compared: random distributed errors and bursts of errors. These errors will be simulated from detections in ECG signals to have a reference to compare with.

1.4 Structure

This dissertation is organized in five chapters, not counting this one.

- The following chapter will explain the context of this work. It will try to answer questions about what the ANS is, what its functions are and why it is important to monitor it in an non-invasive way.
- Chapter 3 is dedicated to materials and methods. It will explain the database and the different preprocessing and HRV methods used.
- Results will be shown in Chapter 4.
- Chapter 5 is dedicated to the discussion, where several issues about methods and results will be addressed
- Finally, Chapter 6 is dedicated to the conclusions.

Chapter 2

Theoretical framework

This chapter provides a brief explanation of the physiological concepts discussed on the following pages: the autonomic nervous system and heart rate variability, as well as their relation.

2.1 Autonomic nervous system

The autonomic nervous system is the division of the nervous system that controls most visceral functions of the body: it can rapidly modify functions such as heart rate, blood pressure, sweating and gastrointestinal motility. Its main function is to assist in maintaining a constant internal environment, a complex process which is called homeostasis [4]. The ANS provides sensory information to the Central Nervous System (CNS, brain and spinal cord) about the situation of the viscera. It is the responsible of evoking feelings like hunger, thirst, or nausea, that helps the organism to maintain homeostasis by voluntary behaviours such as drink or eat.

Although it can evoke this perceptions and behaviours, the main regulation of the ANS is unconscious. Internal stimuli that are collected by different sensors in the viscera lead to a compensatory mechanism, activated mainly by centres in the spinal cord, brain stem and hypothalamus. The ANS can also operate through visceral reflexes, connections that do not need to pass through the brain and therefore act very quickly, triggering subconscious reflex responses [5].

The motor signals returning to the organs (efferent signals) are transmitted by the ANS through two subdivisions, called sympathetic and parasympathetic divisions.

2.1.1 Sympathetic and parasympathetic divisions

Both motor divisions, the sympathetic and the parasympathetic, are connected to the organs through a two-neuron pathway. The first neuron (preganglionic) has its body within the CNS, while the second neuron

(postganglionic) has its body in an autonomic ganglion and it's connected to smooth muscle, cardiac muscle, glands or the walls of the gastrointestinal tract, as depicted in Figure 2.1. Not all tissues are innervated by the two divisions, *e.g.* most of the blood vessels, glands and smooth muscle are only affected by the sympathetic one. Both sympathetic and parasympathetic stimuli can cause inhibitory or stimulating effects, as shown in Table 2.1. However, they usually have antagonistic effects on the same organ: if sympathetic innervation stimulates an effect, normally the parasympathetic will produce an inhibition and vice versa.

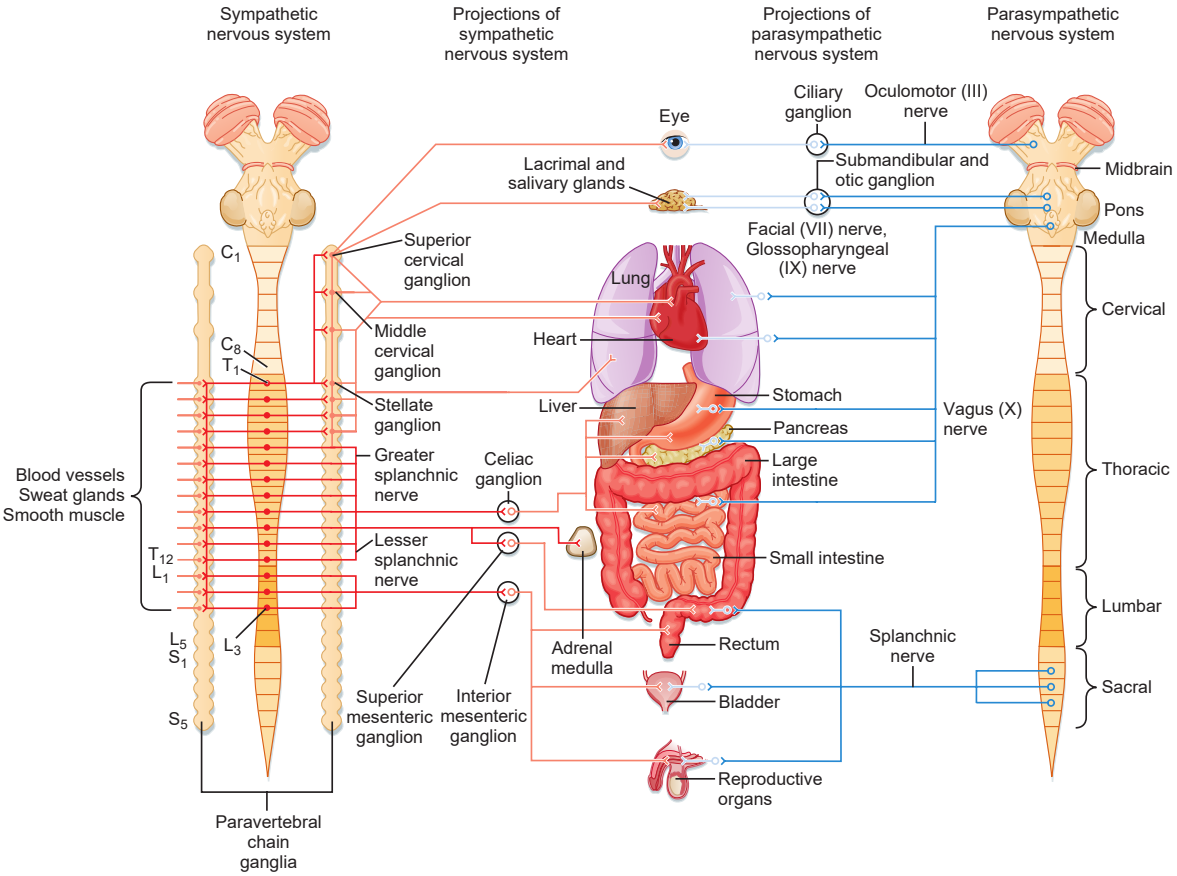

Figure 2.1: Sympathetic and Parasympathetic Pathways (from [4]).

Despite the fact that they often have antagonistic effects (not always), parasympathetic and sympathetic act in a coordinated manner, maintaining internal balance. The examples shown in Table 2.1 may illustrate the idea discussed above that the sympathetic has related a "fight or flight" response while the parasympathetic has a "rest and digest" one. During rest, the prevalence of the parasympathetic tone, maintains a low heart rate and relaxed breathing while stimulating peristaltic movements of the gut and other parts of the gastrointestinal tract, aiding digestion. On the other hand, during a sprint to a bus stop when the bus is about to arrive, the sympathetic tone increases, thus dilating the bronchi in the lungs and increasing the heart rate and contractility,

in order to compensate the demand of oxygen and blood to the tissues. Also the strength of the skeletal muscles is increased and peristaltic movements are inhibited.

Organ	Sympathetic effect	Parasympathetic effect
Pupil	Dilated	Constricted
Heart	Increased rate	Slowed rate
Blood vessels	Most often constricted	Most often little or no effect
Bronchi	Dilated	Constricted
Gut	Decreased peristalsis and tone	Increased peristalsis and tone
Liver	Glucose released	Slight glycogen synthesis
Blood	Increased coagulation	None
Skeletal muscle	Increased glycogenolysis and strenght	None
Kidney	Decreased urine output	None
Glands	Vasoconstriction and slight secretion	Stimulation of copious secretion
Sweat glands	Copious sweating	Sweating on palms of hands

Table 2.1: Autonomic effects on various organs [5].

In spite of these various effects, this thesis will focus only on the control of the heart, specifically on the control of the heart rate, since it allows to perform an autonomic evaluation in a non-invasive way.

2.1.2 Autonomic control of the heart

Some cells in heart tissue have the ability to become self-excited. These cells are mainly concentrated in the SA node, also known as sinus node, located in the wall of the right atrium (see Figure 2.2a). In a physiological case, self-excitation of the SA node cells produces electrical impulses in a rhythmic manner, which are transmitted through fast conduction pathways along the atria. These electrical impulses, called action potentials, cause the atrial muscle to contract, a process known as atrial systole. Blood within the atria is pumped into the ventricles. At this point, the action potential has reached the Atrioventricular Node (AV node), where it is slightly delayed, allowing the atria to be completely emptied. After this short delay, the action potential is rapidly transmitted through the ventricles by the Purkinje system, causing ventricular systole, which pumps blood out of the heart to the tissues. The final phase of the heartbeat is diastole, which consists of heart muscle relaxation and cell repolarization, allowing the cells to be activated by the next action potential to pump again.

Despite the fact that the heart can pump blood automatically - in fact, a heart can beat outside the body due to its ability to self-excite - the human body does not need the same blood supply throughout the day, so it requires a certain control. For example, during emotional excitement or during exercise, the HR increases, while it decreases during sleep. As depicted in Figure 2.2b, the heart is innervated by the sympathetic and parasympathetic divisions of the autonomic system. While the parasympathetic division, through vagi, mainly innervates the SA node and the AV node, the sympathetic division is

distributed along the entire heart. The parasympathetic branch decreases the self-excitation of the cells of the SA node, decreasing HR. It also decreases the excitability of the AV node, increasing the delay at this point, thus extending the duration of the heartbeat. In contrast, the sympathetic branch causes the opposite effects: it increases the HR by stimulating the SA node, and increases the excitability of all the cells in the heart, aiding the electrical impulse transmission. In addition, it enhances the strength of heart muscle contraction.

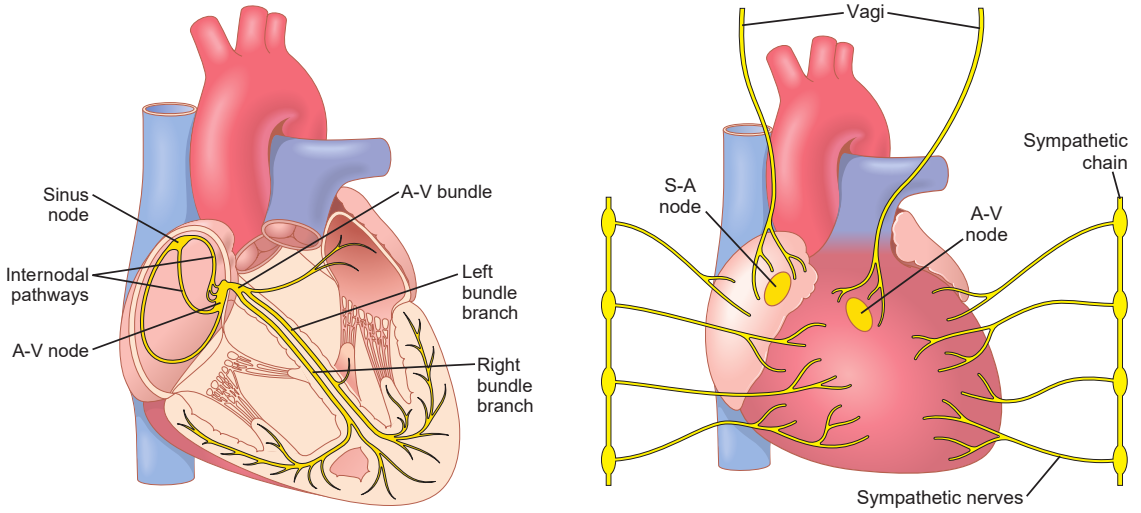

(a) Electrical conduction pathways. **(b)** Autonomic innervation.

Figure 2.2: Cardiac conduction and innervation (from [5]).

Both autonomic stimulations can act very quickly and with clear effects: the parasympathetic can completely stop the rhythmic excitation of the SA node, while the sympathetic can triple the normal HR and double the contraction [5].

2.2 Heart rate variability

Oscillatory patterns of heart rate and blood pressure, and their correlation with respiratory cycle, are known since the 18th century [6]. Later, in the 19th century, cyclical changes in arterial pressure (10-second waves) were discovered by Mayer [7]. However, the broad clinical relevance of heart oscillations around a mean heart rate was not revealed until the 1960s, with the application of computers. Several studies have shown that autonomic monitoring has the ability to predict major body disorders, some of them lethal, that can be prevented with minimally invasive devices and techniques since HRV represents the integrated response of the cardiovascular system to several different influences [8]. In addition, HRV helped to shed light on hitherto poorly understood mechanisms of autonomic control. The following lines describe how information is derived from cardiovascular signals.

Typically, HRV is obtained from the Electrocardiography/Electrocardiogram (ECG). Electrodes on the skin surface measure the electrical activity of the heart, producing the known waveform shown in Figure 2.3. Each phase of the heart cycle is related to a waveform in the ECG. At the beginning of the heartbeat, the atrial systole produces the P wave, followed by a short rest interval corresponding to the delay introduced by the AV node. Once the electrical impulse leaves the AV node, it is transmitted to the ventricles, causing ventricular systole. This can be seen on the ECG as a set of three waves: Q, R and S; usually treated as a single group called QRS complex. Ventricular systole, and therefore the QRS complex, has a very short duration due to the rapid conduction of the Purkinje system; and a large amplitude compared to the P wave due to the greater amount of cells forming the ventricles with respect to the atria. The last waveform, the T wave, is produced by the repolarization of the ventricles during diastole.

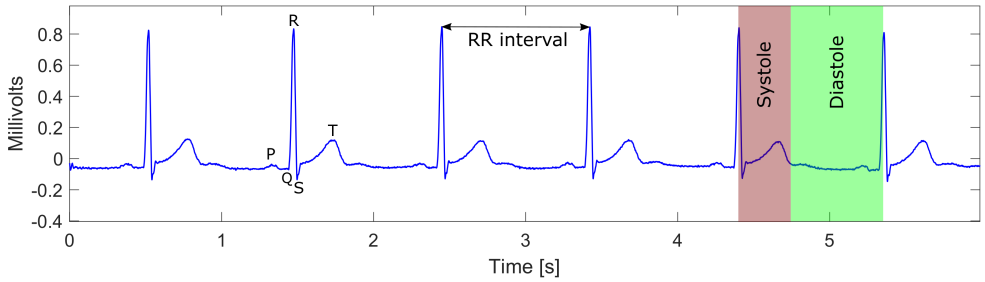

Figure 2.3: Electrocardiogram: Waves, R-R interval and systole/diastole extension.

Although the complete ECG has huge information about the heart, HRV methods rely only on QRS complex detections, which is the easiest wave to detect due to its high energy concentrated in a short time period. Therefore, it represents a reliable reference point of the periodic activity of the heart and its variability. In order to obtain HRV indices, it is necessary to calculate the R-R intervals as the difference between two consecutive R waves (*i.e.* the inverse of the instantaneous heart rate). The representation of this signal is called tachogram (Figure 2.4), where oscillations around a mean value are clearly depicted. Note that the time axis is unevenly sampled due to the variability of the heart rate, and therefore in the sampling rate.

Some variables of interest such as mean heart rate can be calculated directly from the R-R interval series. Measures such as variance indicate aggregated fluctuations of the HR around the mean, thus measuring total power of HRV, regardless of the origin. Despite this limitation, simple time domain parameters are still useful to evaluate HRV. During sympathetic activation the resulting tachycardia is usually accompanied by a marked reduction in total power, whereas the reverse occurs during vagal activation [2]. Tachycardia is reflected in a higher mean HR (*i.e.*, a reduced R-R interval), while reduction in total power can be measured as a reduced variance. In [9], cardiac transplant recipients, and

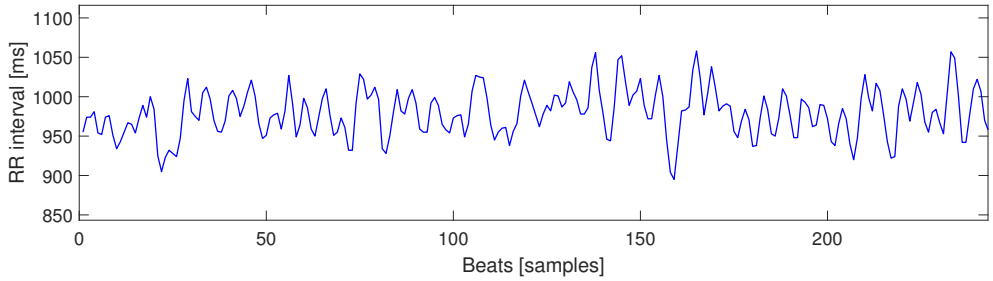

Figure 2.4: Tachogram. The R-R interval physiologically fluctuates around a mean heart rate.

therefore non-innervated hearts, showed a 96% reduction in HRV, demonstrating that heart rate fluctuations were modulated primarily by the ANS. This implies that HRV mainly measures the neural modulations of the ANS.

More interesting variables can be found in the frequency domain. Many methods, which are explained in more detail in the next chapter, can be used to estimate the Power Spectral Density (PSD) either directly from the discrete event series or by interpolating them in order to obtain an evenly sampled signal. This spectrum has an upper limit of approximately half the average heart rate, following the Nyquist-Shannon sampling theorem (around 0.5 Hz). Three components can be distinguished in this band: a Very Low Frequency component (VLF, $< 0.04Hz$); a Low Frequency component (LF, $0.04 - 0.15Hz$), in the same band of arterial pressure cyclic fluctuations (Mayer waves); and a High Frequency component (HF, $0.14 - 0.4Hz$), the same frequencies of Respiratory Sinus Arrhythmia (RSA, *i.e.*, shortened R-R intervals during inspiration and prolonged during expiration). Depending on the respiratory rate, this bounds may not be accurate. This will be addressed on the discussion. The meaning and relation of these components to physiological processes has been widely studied by several investigations since the 1980s, following the path initiated by Akselrod et al. in 1981 [10]. In this research, Akselrod demonstrated, by means of monitoring the effects of selective autonomic blockade in dogs, that the HF component is related to parasympathetic modulation, whereas the LF component is related to both sympathetic and parasympathetic activity, in addition of renin-angiotensin system. This novel approach allowed to distinguish modulations due to each motor division of the ANS in a non-invasive way, previously known by means of invasive methods [11]. Coherent results were found by Pomeranz et al. in humans [12], showing that standing position increase the LF component of HRV from supine values, suggesting a relation between postural movements and autonomic control mediated by blood pressure and baroreflex in this frequency range. They also showed that controlled respiration enhance the HF component, demonstrating its relation with respiration. This increase in the HF component, accompanied with a significant reduction of the LF one was also observed in [13]. In the same decade, Sands et al. discovered that, in cardiac recipients [9], the prominent peak at respiratory rate, *i.e.*, the HF component, was absent

or substantially diminished, suggesting that vagal innervation is a necessary condition for RSA. Despite the efforts made by several researchers, VLF band has not a well defined physiological relation yet, although it is suggested that it is associated with cyclic fluctuations in peripheral vasomotor tone associated with thermoregulation [14]. Furthermore, it requires long recordings where the signal may not be stationary, thus conditioning the spectral estimation.

These researches lead to the conclusion that HRV has 1) a respiratory rhythm, defined as the HF component, which is a marker of vagal modulation; 2) a rhythm corresponding to vasomotor waves, defined as the LF component, which is a marker of both sympathetic and vagal modulations; 3) these rhythms have a reciprocal relation similar to that characterizing the sympathovagal balance [11].

Besides time and frequency-domain metrics, also non-linear and symbolic metrics have been developed in recent times, in order to obtain hidden information from HRV that classic methods are unable to provide. These methods and metrics will be described in the following chapter.

2.2.1 Clinical applications of HRV

Several reviews about HRV have been made, relating many of the methods of the state of the art with pathologies and clinical uses [2, 15]. Some of these studies are commented in the following lines. In [8], it is shown that patients have a depressed HRV early after myocardial infarction, significantly associated with early mortality and major complications and supported by other clinical parameters. The same study states that HRV may reflect haemodynamic damage better than any of the other used parameters. In [16], a spectral analysis over patients surviving an acute myocardial infarction showed an increased LF and diminished HF in normalized units that would indicate a shift of the sympathovagal balance towards sympathetic predominance, revealing alterations in neural control mechanisms. In the previous cited research on cardiac recipients [9], they also found that there was a significant increase in HRV in patients showing histological evidence of rejection. Some diseases like diabetic neuropathy can be preceded by a reduction in time-domain parameters of HRV although without sympathovagal shift, suggesting that both efferent autonomic branches are involved [17]. In [18], it was suggested that patients with essential hypertension has an enhanced sympathetic and a reduced vagal activity, since LF was greater and HF lesser than those observed in the control group. Statistically significant differences in HRV were found in patients with ischaemic heart disease, congestive heart failure and Chagas's disease as stated in [11]. These different situations would not be detectable by simple visual inspection of ECG, proving the importance of computer-mediated HRV in a clinical environment.

2.2.2 HRV and wearables

Non-invasive assessment of the ANS has been extensively researched as a potential tool for the prognosis, diagnosis and monitoring of diseases, mainly in the clinical environment. However, in recent years the market for portable (or wearable) smart devices has boomed, with an increase in their functionality and a decrease in their cost. Because a larger part of the population has easy access to these devices, monitoring the state of the ANS during daily life has become a very attractive objective in the field of health and well-being. A recent study by IDTechEx [19] showed that wrist devices are the most widespread and accepted wearable devices for everyday use. The variety of designs they offer, often camouflaged as watches, has made them an everyday object, allowing non-invasive health monitoring even in the non-patient population.

Traditionally, HRV has been obtained from the electrocardiographic signal which, despite advances in technology, still requires the use of contact electrodes (adhesives, on a strip, on textiles, etc.). This limits their use and acceptance for daily monitoring, particularly by the non-patient population. Although there are different commercial wristband wearables that claim to perform HRV measurements using the photoplethysmographic pulse signal (PPG) on the wrist (which takes the name of pulse rate variabiliy), there are few studies that have validated it with respect to the ECG-derived HRV [20], demonstrating important limitations for robust estimation of classic HRV metrics. Therefore, there is a gap in the market and a need for non-invasive systems, both robust in their estimation of HRV, low cost and accepted by the non-patient population.

There are numerous wrist devices that provide heart rate information, most of them from the PPG signal recorded by a light transmitter and receiver. However, although several studies have validated the HRV obtained from the PPG signal recorded on the finger and forehead [21], very few studies have validated the HRV obtained from the PPG signal recorded on the wrist during daily life. Most studies that extract heart rhythm information from the PPG signal recorded on the wrist only analyze the mean heart rate. However, analysis of HRV requires detection of every single pulse, which is compromised in ambulatory conditions. The proliferation of wearable devices makes it necessary to investigate the degradation of HRV metrics in the face of incomplete recordings, where detections have been lost due to noise and movements.

Chapter 3

Materials and methods

3.1 Database

The database used in this master's thesis has been previously used in [22]. 17 subjects (age 28.5±2.8 years, 11 males) underwent a tilt-table test consisting in 4 min in supine position, 5 min at a 70º angle and 4 min back to supine position. Several signals were recorded, including ECG, blood pressure, oxygen saturation and respiratory signal. The HRV study in this work will use both the respiratory signal and the ECG. Windows of 2 min length are used, where stationarity is assumed [22]. For each phase, windows are selected trying to avoid possible artifacts.

The tilt-table test is a common method used in the clinic to assess the cause of unexplained fainting (syncope). During the test, the patient's heart is monitored by electrodes while it is held in a supine position. The patient rests on a special table that has an automatic mechanism to eventually move into an upright position. This table usually has a footboard and straps to hold the patient. The goal of the test is to trigger symptoms that indicate abnormal control of heart rate or blood pressure, which is necessary in the transition from the supine to the upright position.

It is assumed that the slight tachycardia usually accompanying the upright position is due to a sympathovagal shift towards sympathetic predominance in the neural modulation of the SA node. Enhanced sympathetic drive to the heart is associated with a marked increase in the LF and with a decrease in the HF component of the beat-to-beat R-R variability and arterial pressure [13]. Moreover, the grade of sympathovagal shift is strongly correlated with the degree of tilt, as demonstrated in [23]. In Figure 3.1, it can be shown the effects of the test in a healthy subject. Time-domain measurements indicate an augmented HR during tilt, accompanied with a variability (variance) reduction. Sympathovagal shift is evident in the frequency domain. Although there is an absolute reduction in the power of both LF and HF components, the relative power of each band follows opposite directions as expressed in normalized units

(n.u.). Normalized units are calculated by dividing the power of each band by the sum of the powers of the HF and LF bands, thus excluding the VLF band.

$$P[nu] = \frac{P[ms^2]}{\sigma[ms^2] - P_{VLF}[ms^2]} * 100 \tag{3.1}$$

This representation emphasizes the balanced behavior of the two branches of the ANS, while minimizes the effect of the changes in total power that may mask the sympathovagal shift [2]. The ratio between LF and HF component powers (LF/HF ratio) can complement the information given by the two components separately, taking into account the whole system interaction, thus giving a quantitative index of sympathovagal balance. The increase in the LF/HF ratio during tilt is a consequence of the balance shift towards sympathetic predominance.

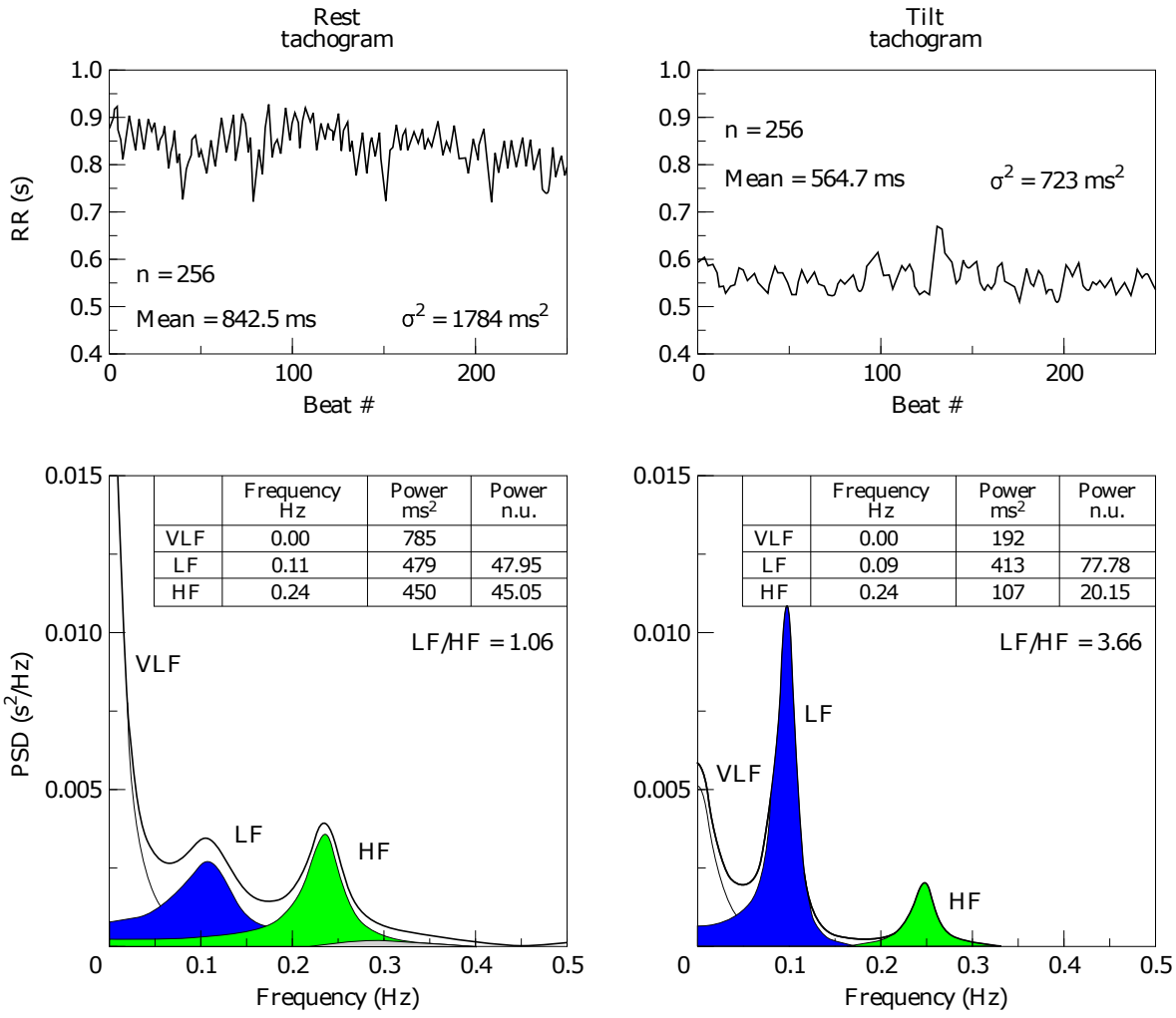

Figure 3.1: Tilt test (adapted from [2]). Tachogram and PSD in supine rest (left) and head-up tilt (right).

Due to its properties, tilt-table test has become a popular method for evaluating sympathovagal balance: passive tilt only entails a minimal engagement of central drive and muscular activity and is compatible with accurate stationary conditions, differing from physical exercise, which is characterized by extreme reductions in HRV, nonlinearities, nonstationarities, and by an enhanced respiratory activity [23]. For these reasons, a tilt-test database is used in this thesis for inducing intra-subjects sympathovagal shifts. Several balance markers will be compared in adverse conditions (*i.e.*, missing beats) in order to determine those with best performance.

3.1.1 R-wave detection

Heartbeats were annotated using a wavelet-based algorithm described in [24]. All the marks have been automatically shifted to the R-wave instants, the signal maxima in according to the lead used (lead IV), and then checked manually, in order to avoid any detection bias in the following steps (see Figure 3.2). At this point, the ECG signal is no longer needed. HRV metrics will be obtained from the time series of beat occurrences for each record.

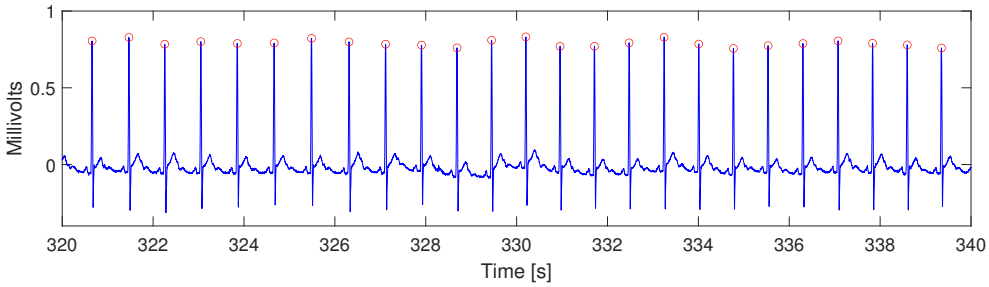

Figure 3.2: Electrocardiogram (lead IV) with marks at R waves.

3.2 Missing data simulation

At this point, there are two windows of 2 minutes per subject, each one characterizing each supine and tilt states. Computations over initial windows yield a reference for each method under review. Later, missed beats are simulated by removing detections directly from the time series. As the objective of this work is to characterize the degradation of the different ANS assessment methods due to missed pulses in the detection stage, simulation permits certain level of losses and a control group using all the detections. Simulation is done in two ways: through a random distribution or through deletion bursts.

3.2.1 Random distribution

This method simulates the effect of a low Signal to Noise Ratio (SNR). Sometimes, signals have enough quality to perform detections, although an

automatic detector can still miss some pulses (see Figure 3.3). In fact, they can find pulses where there are none, but that case is not investigated in this thesis. This is achieved using a binomial distribution with different probabilities, so every pulse can be deleted or not with a p probability (*i.e.*, every pulse deletion is an independent Bernoulli trial). Different number of pulses are eliminated in each series, depending on the mean heart rate. However, the proportion of removed pulses will be the same.

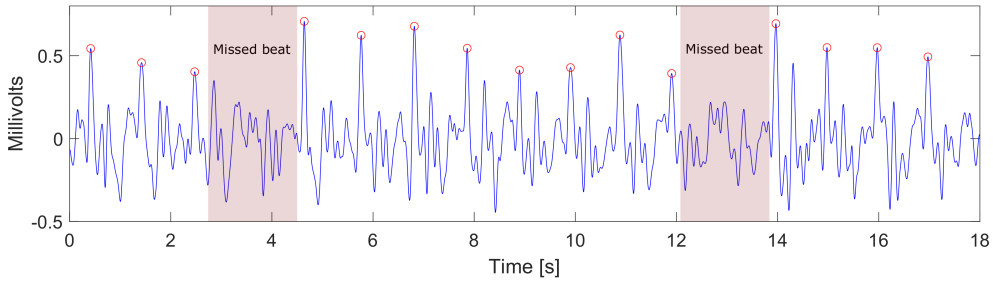

Figure 3.3: Noisy ECG with random missed beats. R-wave detections are marked with red circles.

3.2.2 Bursts

On the other hand, signals with a high SNR can be affected by artifacts. This kind of noise is mainly caused by movements and is characterized by a finite duration and a total loss of the signal or a very low SNR. These events cause a burst of missed detections, rather than those randomly distributed (see Figure 3.4). It is a common problem in wearables. This effect has been simulated by removing pulses from the center of the series to each side with windows of a certain duration.

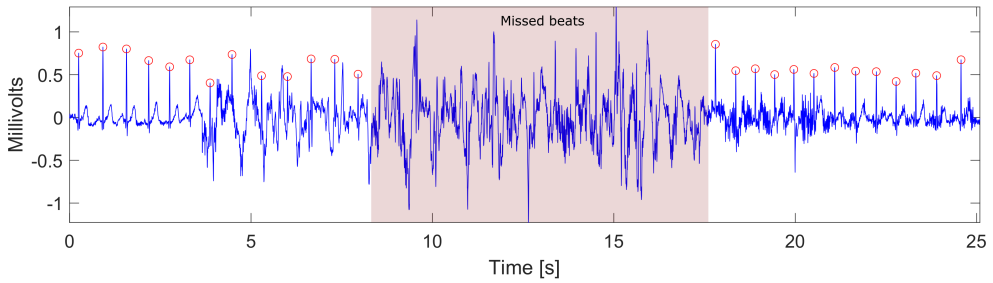

Figure 3.4: ECG with a burst of missed beats due to artifacts. R-wave detections are marked with a red circle.

3.3 Missing data detection

Some methods require missing pulses to be detected. This is a relatively simple task when the error rate is low or distributed in bursts. It is sufficient

to look for sharp increases in the R-R interval series that suggest that at least one heartbeat is missing between two pulses. However, this task become more complicated when errors are randomly distributed and their number begins to grow, as the reference R-R is lost. A moving median threshold is used in all methods to detect these jumps in the R-R series. This method also allows the detection of false positives and ectopic beats, either by placing a lower threshold (a false positive causes a sudden drop in the R-R interval), or by applying the threshold to the absolute value of the series of differences in the R-R intervals. In the case of missing pulse bursts, the R-R series will have only one outlier at the end of the burst. It is very easy to detect even with fixed thresholds (e.g. two seconds). The larger the bursts, the easier it is to distinguish the outlier from the baseline. Once the gaps have been identified, two possible techniques are proposed to deal with them. The first is to eliminate these outliers from the R-R series. As some methods may present a strong degradation due to incomplete R-R series, the second technique is to fill the gaps in with approximate pulses inferred from the surrounding actual ones. The way this is done is explained in the next section.

3.4 Filling in the gaps

Different insertion methods may be used to fill the gaps in. The ectopic heartbeat corrector described in [25] is an excellent approach for small amounts of missed detections and ectopic beats. First, when a gap is detected between pulses t_k and t_{k+1}, the algorithm tries either to insert an intermediate beat; to move t_k to a intermediate position between t_{k-1} and t_k; or to move t_{k+1} to the intermediate position between t_{k+1} and t_{k+2}. Then, the threshold condition is checked with the new series. If the condition is not met at any of the situations, it is extended by considering possible consecutive missed beats (two consecutive insertions or movements), and so on until the condition is satisfied by involving one more beat in each step. The criterion is to solve the anomaly by modifying the minor number of original beats. It also tries to meet the condition removing beats in order to deal with false positives or ectopic beats. The main problem with this method for use as a gap-filling method is that it has difficulty distinguishing how many pulses are missing from each gap. By allowing it to move the pulses instead of forcing it to introduce new ones, it often causes the solution to have a different number of beats than the actual ones. This difference in the number of pulses may not affect methods that interpolate the series before, such as some frequency methods, since it produces smooth series. However, other methods such as temporal methods where the series are not interpolated, will suffer some degradation. From now on this method will be called the **reference method**.

A second method is proposed to overcome this problem, using an iterative algorithm. First, it starts by interpolating the series with a single pulse per gap

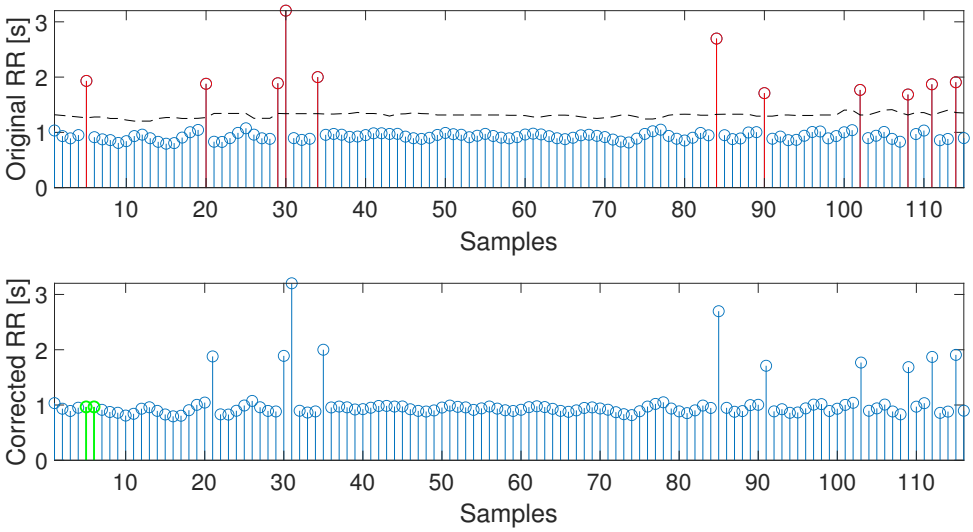

(a) Small gaps are filled first. *Above*: Original RR series. The moving median threshold is represented by a dashed line. R-R intervals above the threshold (in red) have to be modified. *Below*: First gap successfully corrected in the first iteration.

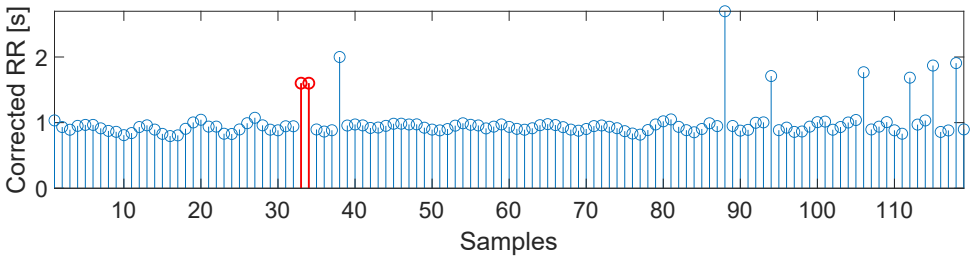

(b) A gap larger than a pulse still exceeds the threshold after correction. It will have to be filled in during the subsequent iterations.

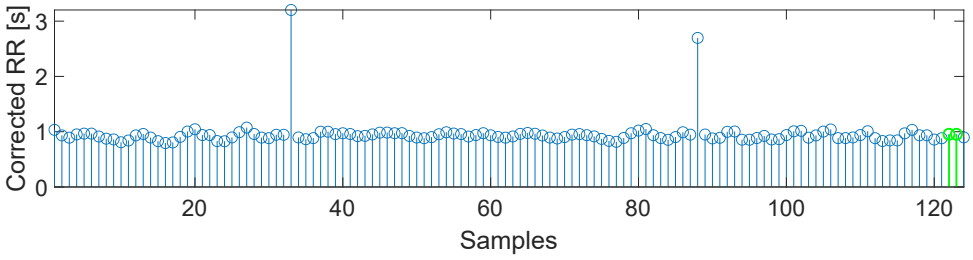

(c) First iteration concluded. Most of the gaps are corrected but there are still gaps. Another iteration will be necessary.

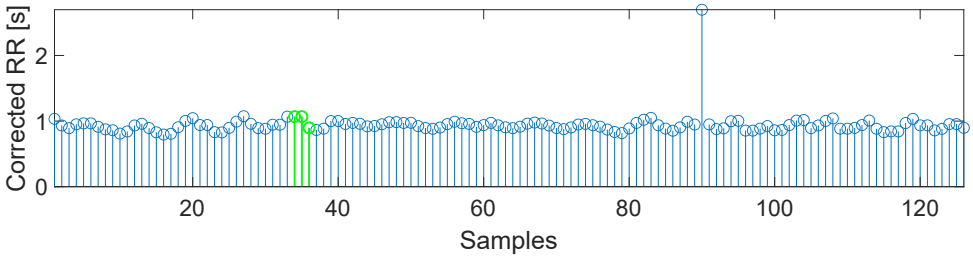

(d) Now the number of filling pulses is correct. The algorithm will continue to fill gaps until no R-R interval exceeds the threshold.

Figure 3.5: Iterative method demonstration.

(Figure 3.5a). Then, it is checked if the number of missing pulses was correct by checking with the same moving median method if the threshold is exceeded. For cases where there is still a peak (Figure 3.5b), the introduced pulse is eliminated and the algorithm continue with the subsequent gaps (Figure 3.5c). A two-pulse interpolation is tested in the following iteration (Figure 3.5d), and so on. The use of an iterative algorithm aims to solve two problems of pulse correction: the complication of distinguishing the reference series from the gaps and the lack of knowledge of the number of pulses missing from each gap. Thus, it starts by solving the "simple" gaps before those involving more than one pulse. The interpolation method will greatly affect the results. Here, linear interpolation is used. Interpolation methods with higher order polynomials, including cubic splines, may have convergence problems by introducing unwanted oscillations. From now on this method will be called the **proposed method**.

3.5 Time-domain metrics

Time-domain methods are the easiest and most direct to implement, since they are simple statistical analysis performed directly on the series of R-R intervals or on the differences between intervals. The simplest is probably the **mean heart rate (MHR)**, calculated as the mean of the inverses of the R-R series. It is an important marker, since it is directly related to the degree of activation of the sinus node. Also it is an accurate metric even from very short segments (less than 1 min) [26].

Another easy to calculate metric is the **standard deviation of the N-N interval (SDNN)**. The N-N interval is the interval between QRS complexes produced by depolarization of the sinus node, *i.e.* the R-R intervals after ectopic heartbeats have been eliminated. This measure is equivalent to the square root of the variance, so it is a measure of the total power of the variability. Therefore, it also does not allow an assessment of what division of the autonomous system is causing it.

Among the metrics that allow for better discrimination of the components of variability are: the **square root of the mean squared differences of successive NN intervals (RMSSD)**, the **standard deviation of successive differences (SDSD)** and the **proportion of successive intervals that differ by more than 50 ms (pNN50)**. They are all calculated from the difference between intervals instead of from the R-R interval series itself. Since they all measure in some way the magnitude of the changes, they all measure the speed at which variability occurs. Therefore they are are roughly related to the HF band of the spectrum and correlated with each other.

As time-domain metrics are computed over the R-R interval series, gaps will produce a degradation by introducing outliers. The metrics will be computed both without preprocessing, removing outliers, and filling in the gaps with both the reference and proposed methods. In the case of removing outliers without

interpolation, the outliers should be removed both in the R-R and the successive differences series.

3.6 Frequency-domain metrics

As seen in the previous chapter, frequency analysis allows the separation of neural control of the HRV into separate components. In particular, the LF (0.04-0.15Hz) and HF (0.15-0.4Hz) bands are of interest for ANS characterization. Regardless of the method for calculating the spectrum, only estimates can be obtained. Methods are generally classified into parametric and non-parametric. Non-parametric methods have the advantage of being simple to implement and very fast to execute. They are usually based on Fast Fourier Transformation (FFT). On the other hand, parametric methods produce smoother and easier to process spectra [2]. The different components are already separated and have a central frequency identified. Another major advantage is that they produce an accurate estimate of the PSD with a small number of samples. This is why they might be more suitable in a lossy environment like the one under study. On the other hand, the order of the model, usually an autoregressive model, has to be correctly estimated. Spectral estimation has been realized in this work via Welch's method, Lomb's method and AR models. One example for each method is shown in Figure 3.6. Note that there are significant differences between estimates from the same recording.

As the HF component is related to respiratory rhythms, the classic 0.15-0.4Hz band may not be accurate for all the cases. It is assumed that respiratory rate is usually within this range but, in some cases, like supine rest, it may be out of these bounds. If the respiratory rate is too low, the HF component would overlap the LF one and the sympathetic and parasympathetic contributions would not be distinguishable from the aggregate variability. For a correct frequency separation, only subjects with respiratory rates within the HF band (RR> 0.15Hz, 9 breaths per minute) have been used when the ability to distinguish sympathovagal balance is measured (*i.e.*, all subjects are included when measuring metric degradation, but only those with a respiratory rate within the classic HF band are included when comparing supine and tilt groups), which reduces the population from 17 to 10 subjects. It has also been checked that the respiratory rate does not exceed 0.4Hz in any case, which is the case for all subjects. Four frequency metrics are computed: the **LF and HF power (P_{LF},P_{HF})**, **LF power measured in normalized units (P_{LFn})**, *see Equation* (3.1); and the ratio between LF and HF power (**LF/HF ratio**).

3.6.1 Welch´s method

Since Fourier-based methods expect evenly sampled signals, estimations are made on the of the instantaneous R-R signal ($d_{RR}[n]$, evenly sampled) obtained from the IPFM model [27]. This model assumes that the actions of the autonomic

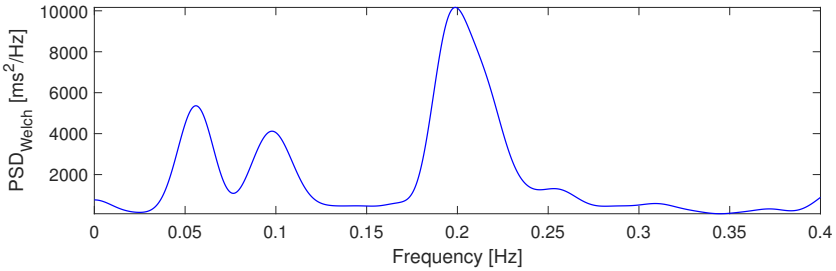

(a) PSD estimate obtained via Welch's method.

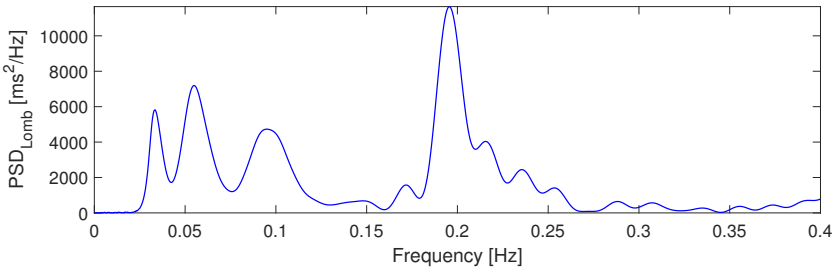

(b) PSD estimate obtained via Lomb's method.

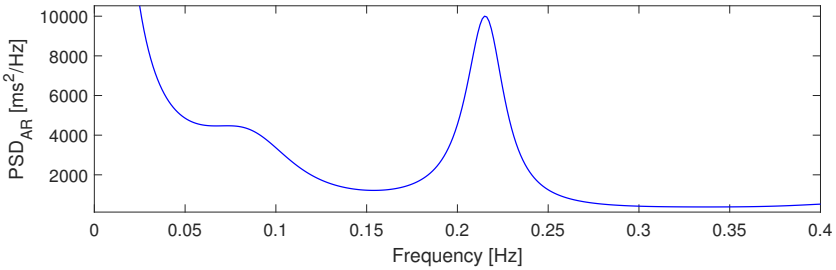

(c) PSD estimate obtained using an AR model.

Figure 3.6: PSD estimates from the same record using different methods.

nervous system on the sinoatrial node can be represented as a band-limited zero-mean modulating signal $m(t)$, and that pulses are triggered when the integral of this function reaches a threshold. For the kth heartbeat:

$$k = \int_0^{t_k} \frac{1 + m(t)}{T} dt \tag{3.2}$$

t_k is the time occurrence of the beat, and T the mean of the R-R intervals. In [28] it is shown that this method yields more reliable spectra than those estimated on the interpolated R-R series using classic interpolation methods such as splines directly on the series, avoiding spurious components and low-pass filtering effects. In addition, it permits the interpolation of the R-R series when these include gaps as described in [25]. However, gaps must be detected before. Welch's method will be tested both detecting the gaps and filling in the pulse series with the reference and proposed methods.

Welch's method is a non-parametric method that estimates the spectral density of a signal by means of periodogram averaging (Figure 3.6a). As the PSD of a signal is the Fourier transform of its autocorrelation function, the periodogram is defined as the Fourier transform of the biased estimate of the

autocorrelation sequence. For a signal $d_{RR}[n]$ of length N, the periodogram $S(f)$ is computed as

$$S(f) = \frac{1}{N}\left|\sum_{n=0}^{N-1} d_{RR}[n]e^{-j2\pi fn}\right|^2 \tag{3.3}$$

Averaging is performed by computing N_{per} periodograms per signal using 60-second Hamming windows with 50% overlap (Equation (3.4)). This allows a reduction in the variance of the estimate at the cost of lower spectral resolution. For 120-seconds signals: $N_{per} = 3$. Powers are computed using trapezoidal integration and classic windows (0.04-0.15Hz for LF and 0.15-0.4Hz for HF).

$$S_{Welch}(f) = \frac{1}{N_{per}}\sum_{i=1}^{N_{per}} S_i(f) \tag{3.4}$$

3.6.2 Averaged Lomb´s method

Lomb PSD estimation method also makes use of Lomb's periodograms, a non-parametric spectral estimation based on a least-squares fit of sinusoids (sin and cos rather than Fourier's exponentials) to data samples [29]. The main advantage of this method is that it can be used directly on the unevenly sampled R-R series ($RR[t_n]$), without the need for filling in the gaps. Lomb's periodogram is computed as

$$S_{Lomb}(F) = \frac{[\sum_{n=1}^{N}(RR[t_n]-\overline{RR})\cos(2\pi F(t_n-\tau))]^2}{2\sigma^2\sum_{n=1}^{N}\cos^2(2\pi F(t_n-\tau))} + \frac{[\sum_{n=1}^{N}(RR[t_n]-\overline{RR})\sin(2\pi F(t_n-\tau))]^2}{2\sigma^2\sum_{n=1}^{N}\sin^2(2\pi F(t_n-\tau))} \tag{3.5}$$

where the value of τ is defined as

$$\tan(4\pi F\tau) = \frac{\sum_{n=1}^{N}\sin(4\pi F t_n)}{\sum_{n=1}^{N}\cos(4\pi F t_n)} \tag{3.6}$$

being $\overline{RR}$ and σ^2 the mean and variance estimates of $RR[t_n]$ respectively. Although in the case of accurate detections the IPFM model has demonstrated to outperform Lomb's [28], it may be more reliable in case of missing data, as no gap correction is needed and estimation is based only in actual pulses (although it is necessary to eliminate outliers from the R-R series produced by missing data). However, both proposed insertion methods will be tested as well. Lomb's periodograms are averaged using 60-second Hamming windows with 50% overlap as well. The average is realized using the same formula (Equation (3.4)). Powers are computed using trapezoidal integration and classic windows as well.

The oscillatory pattern that appears at the estimate is remarkable (Figure 3.6b) in comparison with the smooth spectra produced by the other two methods. However, since HRV metrics are integral indexes of the spectrum, no substantial effects will be induced in opposition with the low-pass filtering induced by interpolation [29].

3.6.3 Autoregresive model

This is a parametric method where the R-R interval series is modeled as the output of a causal, all pole, discrete filter of order P whose frequency response is

$$H(z) = \frac{1}{1 + \sum_{k=1}^{P} a_k z^{-1}} = \frac{1}{\prod_{k=1}^{P} (1 - p_k z^{-1})} \tag{3.7}$$

and whose input is white noise ($w[i]$) of variance equal to σ^2 [15]:

$$RR[i] = -\sum_{k=1}^{P} a_k RR[i-k] + w[i] \tag{3.8}$$

The model can be characterized by its parameters $\{a_1, a_2, ..., a_P, \sigma^2\}$. Akaike's criterion is used to find the optimal order. Once the parameters are fitted, the power spectrum (Figure 3.6c) is computed as:

$$S_{AR}(f) = \sigma^2 H(z) H^*(1/z^*) = \frac{\sigma^2}{|1 + \sum_{k=1}^{P} a_k e^{-j2\pi f k}|^2} \tag{3.9}$$

In this method the R-R series are indexed by beat order rather than by beat occurrence time. The sampling frequency is approximated as the inverse of the average R-R interval. However, it does require that the gaps be filled, so both reference and proposed methods are used. Powers are not calculated integrating the spectra as in non-parametric methods. Decomposition of the spectrum using partial fraction expansion is performed instead [1]. P_{LF} and P_{HF} are computed as the associated power to all partial spectra whose central frequency is within the classic bands, using the residue theorem.

3.7 Poincaré plots

Poincaré plots are graphic methods of representing interbeat dynamics. Each RR interval is represented as a function of the previous RR interval, generating a scatterplot that represents the phase space of the series (Figure 3.7a). Poincaré plots have become an integral part of HRV analysis, where they are shown to provide prognostic information in myocardial infarction, chronic heart failure, and sudden infant death syndrome [30]. Recently, Poincaré plots reliability has been demonstrated in ultra-short term monitoring (less than 5 minutes) [31]. The problem regarding Poincaré plots is the lack of obvious quantitative

measures that characterize the salient features of the plot. Here, the ellipse fitting method (Figure 3.7b) has been chosen. An ellipse is adjusted to the data shape and geometric indexes are extracted. These indexes are:

- **SD1**: the standard deviation of the points projection on the ellipse axis perpendicular to the line-of identity. This measure is related to the fast beat-to-beat variability.
- **SD2**: the standard deviation of the projected points along the line-of identity, that measures long term dynamics of HRV.
- **SD1/SD2**: the ratio, to describe the relationship between these components.
- **S**: the area of the ellipse. $S = \pi \cdot SD1 \cdot SD2$.
- **Md**: the mean data distance to the ellipse centroid (Euclidean norm).
- **Sd**: the standard deviation to the ellipse centroid (Euclidean norm).

This technique will be tested both without preprocessing, eliminating the outliers, and filling in the gaps by both proposed methods.

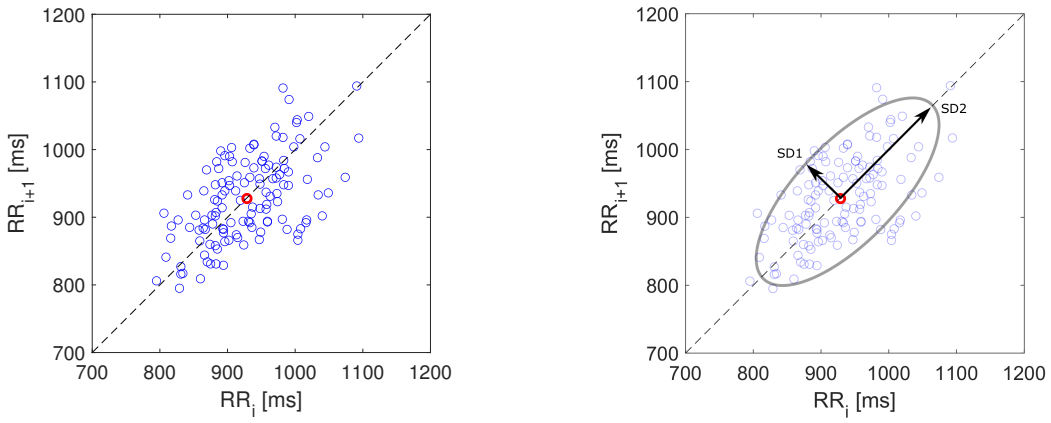

(a) Original. **(b)** Ellipse fitting method.

Figure 3.7: Lagged Poincaré plots.

3.8 Symbolic metrics

A novel approach for the analysis of short-term HRV have recently appeared. Costa *et al.* [32, 33] have developed a new method termed Heart Rate Fragmentation (HRF), based on beat-to-beat R-R interval acceleration direction (whether the R-R intervals increase or decrease) rather than its absolute values. Based on this, they propose the following metrics:

- **Percentage of inflection points (PIP)**: A beat represents an inflection point if is an instant of inversion of heart rate acceleration sign (from acceleration to deceleration or vice versa). The higher the PIP, the higher the fragmentation.
- **Inverse of the average length of the acceleration/deceleration segments (IALS)**: The length of a segment is the number of R-R intervals between consecutive inflection points.
- **Percentage of short segments (PSS)**: Proportion of segments having only one or two R-R intervals over total segments.
- **Percentage of R-R intervals in alternation segments (PAS)**: An alternation segment is a sequence of at least four R-R intervals, for which heart rate acceleration changes sign every beat.

Both insertion methods will be tested to compare degradations against no preprocessing.

3.9 Statistical analysis

The Root Mean Square Error (RMSE) is computed to obtain a quantitative measure of the degradation. Sometimes the RMSE will be calculated as a normalized value by dividing the RMSE by the mean value of the metric without degradation. Also, a Wilcoxon signed rank test is used to obtain a measure of the degradation of HRV metrics, allowing to assess whether changes are significantly different. A level of significance of 0.05 is used. Results have been computed with tilt and supine together, pairing records from the same subject for different input degradations. In this way, it is intended to observe degradations when detection errors increase. On the other hand, for autonomic discrimination results, the Wilcoxon test is computed over supine and tilt records as separate samples, pairing supine and tilt estates from the same subject.

Chapter 4

Results

4.1 Randomly distributed missed beats

4.1.1 Time-domain metrics

Metric	Missing beats [%]				
	5	10	15	20	25
MHR [bpm]	1.52	3.38	5.84	8.74	10.50
SDNN [ms]	154.15	265.70	363.88	446.89	578.34
SDSD [ms]	232.49	399.79	552.87	679.51	864.46
RMSSD [ms]	231.54	397.95	550.11	675.83	859.56
pNN50 [%]	6.05	13.65	22.18	31.52	36.71

(a) Without preprocessing.

Metric	Missing beats [%]				
	5	10	15	20	25
MHR [bpm]	0.15	0.23	0.32	0.39	0.39
SDNN [ms]	2.10	2.76	3.40	4.53	4.31
SDSD [ms]	1.37	2.53	3.33	4.23	4.35
RMSSD [ms]	1.35	2.49	3.29	4.20	4.41
pNN50 [%]	1.27	1.93	2.55	3.80	3.46

(b) Removing outliers.

Metric	Missing beats [%]				
	5	10	15	20	25
MHR [bpm]	0.14	0.26	1.53	1.66	1.20
SDNN [ms]	2.91	3.66	78.17	82.38	85.19
SDSD [ms]	5.51	6.94	19.71	26.37	38.02
RMSSD [ms]	5.49	6.91	19.70	26.29	37.82
pNN50 [%]	2.96	6.14	7.61	8.17	8.39

(c) Filling gaps with the reference method.

Metric	Missing beats [%]				
	5	10	15	20	25
MHR [bpm]	0.10	0.14	0.16	0.27	0.46
SDNN [ms]	0.57	1.23	1.89	3.28	5.12
SDSD [ms]	1.80	2.25	2.08	5.54	5.59
RMSSD [ms]	1.80	2.24	2.08	5.52	5.56
pNN50 [%]	1.39	2.33	3.47	4.46	4.99

(d) Filling gaps with the proposed method.

Table 4.1: Degradation of time-domain metrics (RMSE) when missing beats are randomly distributed.

Tables composing Table 4.1 present the degradation of time-domain metrics in terms of root mean square error when missing beats are randomly distributed. The need for some kind of preprocessing becomes evident in Table 4.1a, even for low error rates. A RMSE of 10 beats per minute in MHR is a very important deviation, since it is a metric that in this database varies between 40 and 100 beats per minute. Metrics related to beat-to-beat variability, SDNN, SDSD and RMSSD, have errors more than double the duration of a QRS complex, which is 60 to 100ms, with only a 5% of missed beats. Therefore, the use of these metrics in noisy environments without preprocessing is not recommended. Removing outliers (Table 4.1b) seems to be a robust technique for all the metrics. The errors fall two orders of magnitude with respect to the errors

without preprocessing except for pNN50, which falls only one. All errors are one order of magnitude below the order of the metrics. Figure 4.1 shows the distribution differences of the metrics and Wilcoxon results in the best scenario, *i.e.*, removing outliers without any interpolation. Results are presented by box plots, using green boxes for metrics obtained from supine records and blue boxes from tilt ones. An asterisk (*) indicates p-values lower than 0.05. Two asterisks (**) mark p-values lower than 0.025. These distributions should be as different as possible in order to distinguish the states, so asterisks are desirables.

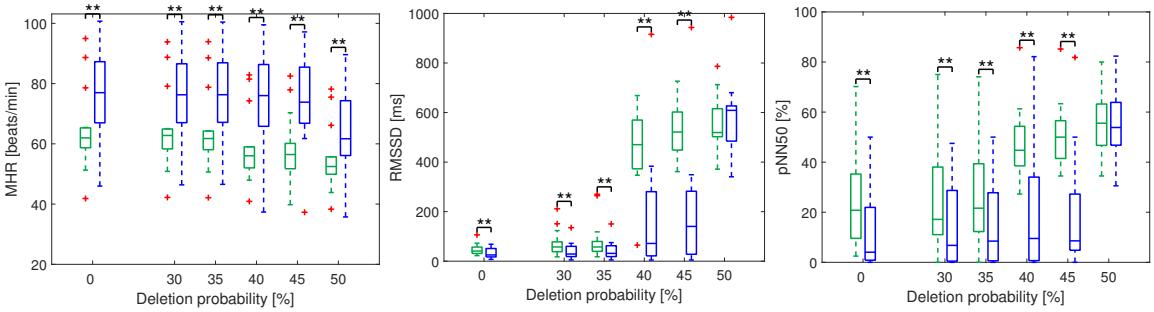

(a) MHR. **(b)** RMSSD. **(c)** pNN50.

Figure 4.1: ANS discrimination of time-domain metrics removing outliers (without interpolation) when missed beats are randomly distributed. Green for supine, blue for tilt.

- MHR: Although it is the only metric that presents significant degradation in median (*i.e.*, p-values below 0.05 for the same recordings with different degradations), it is clearly the most robust metric, as its RMSE never exceeds a heartbeat per minute. A clear increase in the mean heart rate from the supine to the tilted position can be seen at a glance, which is confirmed by the Wilcoxon test with a p-value of less than 0.025. This test allows to distinguish significant differences with up to 60% of randomly distributed missed pulses.

- SDNN, SDSD, RMSSD: In all cases the error is much lower than the duration of an average QRS complex, so the variation of these metrics could be compared to the inaccuracy produced by a pulse detector. In terms of their ability to discriminate the autonomic nervous system variation, both SDSD and RMSSD behave similarly and are able to distinguish states with up to 45% of pulses missing, since there is a reduction in tilted position (remember that SDSD and RMSSD are associated with HF variability). On the other hand, SDNN is not able to discriminate in any case.

- pNN50: It is a reliable measure both in value and in its ability to distinguish states with up to 45% detection loss. The percentage of high variation intervals is lower in the tilted position.

On the other hand, filling gaps does not improve results with respect to the outlier-free case (Tables 4.1c and 4.1d), although the proposed method suffers

a similar degradation for low missed pulse rates. Figure 4.2 shows that this method fail for higher rates, specially above a 35%.

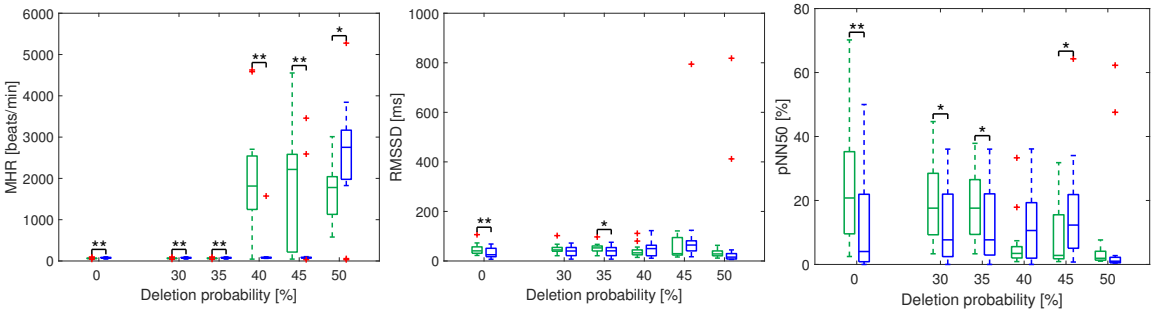

(a) MHR. **(b)** RMSSD. **(c)** pNN50.

Figure 4.2: ANS discrimination of time-domain metrics filling in the gaps with the proposed method when missed beats are randomly distributed. Green for supine, blue for tilt.

The good results, simplicity and low cost of the moving median method without applying interpolation make it the most recommendable technique.

4.1.2 Welch's method

Metric	Missing beats [%]				
	5	10	15	20	25
P_{LF}	0.342	0.356	3.012	4.374	12.741
P_{HF}	0.405	0.484	0.782	3.576	19.976
P_{LFn}	0.046	0.057	0.198	0.238	0.243
P_{LF}/P_{HF}	0.944	2.433	2.811	3.351	4.538

(a) Detecting gaps.

Metric	Missing beats [%]				
	5	10	15	20	25
P_{LF}	0.204	0.234	3.443	5.180	8.458
P_{HF}	0.395	0.483	0.654	1.680	3.247
P_{LFn}	0.051	0.071	0.207	0.265	0.272
P_{LF}/P_{HF}	0.937	2.136	3.959	4.639	4.371

(b) Filling gaps with the reference method.

Metric	Missing beats [%]				
	5	10	15	20	25
P_{LF}	0.076	0.095	0.162	0.251	0.264
P_{HF}	0.084	0.170	0.215	0.360	0.290
P_{LFn}	0.013	0.020	0.032	0.080	0.085
P_{LF}/P_{HF}	0.390	0.398	0.580	1.142	1.838

(c) Filling gaps with the proposed method.

Table 4.2: Degradation of Welch's metrics (RMSE) when missing beats are randomly distributed. RMSE is normalized for P_{LF} and P_{HF}.

Table 4.2 shows the degradation of Welch's method metrics when missing beats are randomly distributed. The proposed method for filling gaps (Table 4.2c) outperforms both the reference method (Table 4.2b) and the case detecting gaps (Table 4.2a). Note that RMSE is normalized for P_{HF} and P_{LF} as is not trivial to understand the magnitude of the degradation in ms^2.

Figure 4.3 shows an example for each method of how the spectra undergo controlled degradation with increasing loss rates. Interpolation could be the cause of a low-pass effect that can be observed in the spectra as a lower HF peak with increasing loss rate, while LF is not systematically affected. This is consistent with an increasing RMSE error of the LF to HF ratio when the loss rate

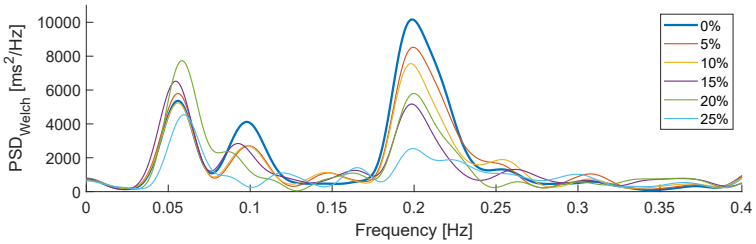

(a) Detecting gaps.

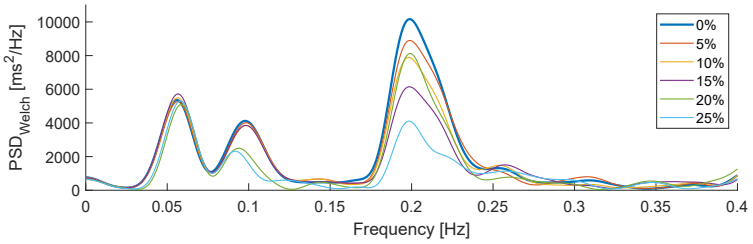

(b) Filling gaps with the reference method.

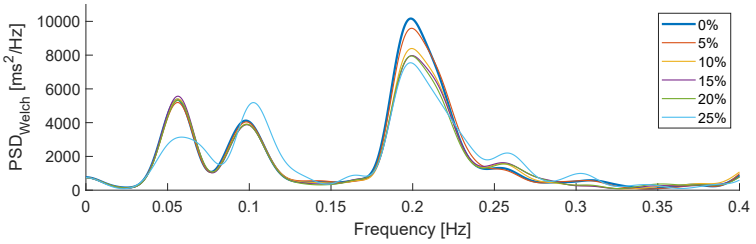

(c) Filling gaps with the proposed method.

Figure 4.3: Welch's spectral estimates from the same record with different loss rates randomly distributed.

is incremented. The proposed method seems to be more robust against this effect and is reflected in both a lower decay of the HF peak and a lower error in the LF/HF ratio.

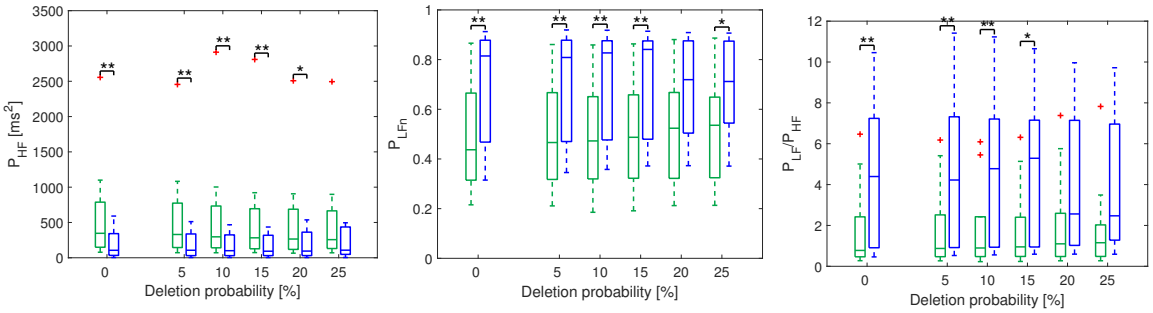

(a) P_{HF}. **(b)** P_{LFn}. **(c)** P_{LF}/P_{HF}.

Figure 4.4: ANS discrimination of Welch's metrics filling in the gaps with the proposed method when missed beats are randomly distributed. Green for supine, blue for tilt.

Figure 4.4 shows the statistical results of the metrics obtained by the proposed method. There is no significant degradation in median for the normalized LF power and the LF/HF ratio distributions even with a 25% of missing beats. Both these metrics and the power in the HF band are also robust in discriminating between ANS states (up to 15-20% of missing beats). P_{LF} cannot

differentiate groups. P_{HF} and P_{LF} estimates are significantly different from their reference value (0% missing beats) for all percentages of data loss.

4.1.3 Averaged Lomb's method

Metric	Missing beats [%]				
	5	10	15	20	25
P_{LF}	0.100	0.179	0.305	0.465	0.583
P_{HF}	0.284	0.520	0.985	1.594	1.998
P_{LFn}	0.048	0.099	0.143	0.189	0.221
P_{LF}/P_{HF}	2.024	2.806	3.378	3.717	4.034

(a) Removing outliers.

Metric	Missing beats [%]				
	5	10	15	20	25
P_{LF}	0.163	0.235	1.706	2.784	3.930
P_{HF}	0.319	0.441	4.288	12.256	14.115
P_{LFn}	0.042	0.072	0.174	0.212	0.218
P_{LF}/P_{HF}	0.747	1.041	2.213	2.748	3.401

(b) Filling gaps with the reference method.

Metric	Missing beats [%]				
	5	10	15	20	25
P_{LF}	0.088	0.149	0.156	0.230	0.259
P_{HF}	0.099	0.121	0.202	0.349	0.331
P_{LFn}	0.014	0.026	0.034	0.082	0.086
P_{LF}/P_{HF}	0.586	0.627	0.577	1.345	1.807

(c) Filling gaps with the proposed method.

Table 4.3: Degradation of Lomb's metrics (RMSE) when missing beats are randomly distributed. RMSE is normalized for P_{LF} and P_{HF}.

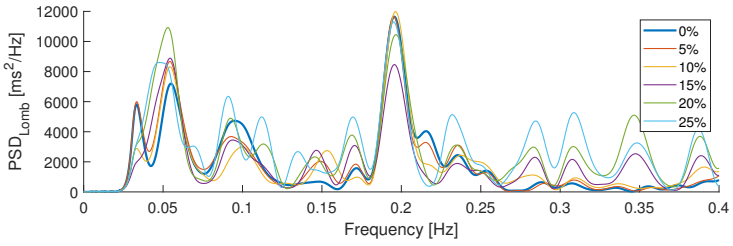

(a) Removing outliers.

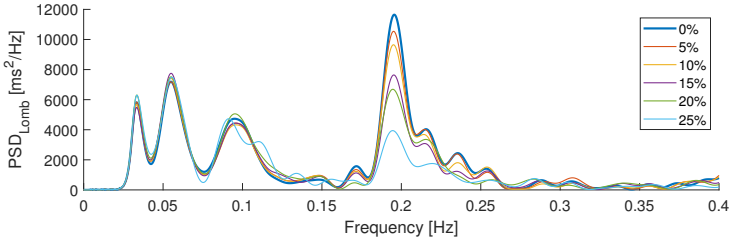

(b) Filling gaps with the reference method.

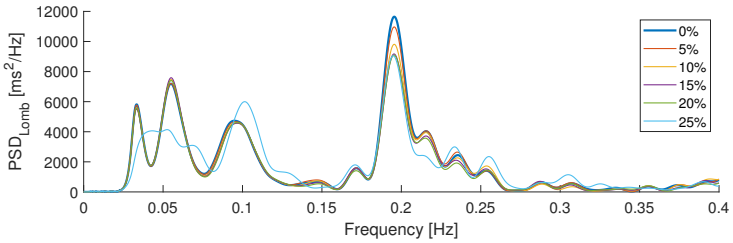

(c) Filling gaps with the proposed method.

Figure 4.5: Lomb's spectral estimates from the same record with different loss rates randomly distributed.

Again, the proposed method has the least amount of error (Table 4.3), achieving a better frequency independence that can be seen in a lower error in the LF/HF ratio. Errors are similar to Welch's. This does not mean that they are equally good estimates, but that they degrade similarly.

Figure 4.5 shows the spectra produced by each preprocessing technique, where the effects are also similar to those of Welch. The main difference is the overshoot that appears in the case without filling any gaps. This effect becomes more evident as fewer samples are available to calculate the spectrum. Therefore, it is not recommended to use this method without interpolation. This will be especially important in the case of bursts. Again, the low-pass effect of the reference method appears prominently, visible both quantitatively as a large error in P_{HF} and visually in the decrease of the HF peak in the spectrum.

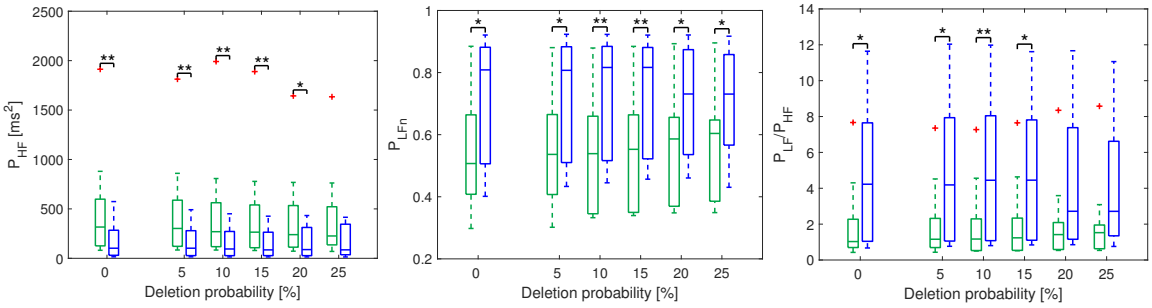

(a) P_{HF}. **(b)** P_{LFn}. **(c)** P_{LF}/P_{HF}.

Figure 4.6: ANS discrimination of Lomb's metrics filling in the gaps with the proposed method when missed beats are randomly distributed. Green for supine, blue for tilt.

Figure 4.6 shows the results of the Wilcoxon test for the proposed method. Neither P_{LFn} nor the LF/HF ratio undergoes significant degradation from their reference values up to 25% of pulses missing while P_{LF} and P_{HF} shows significant degradations from a 5%. P_{LFn} is able to distinguish the states of the ANS with up to 25% of pulses missing. In this sense, the results are also similar to those obtained by Welch. P_{LF} cannot differentiate groups.

4.1.4 AR model

Metric	Missing beats [%]				
	5	10	15	20	25
P_{LF}	0.241	0.382	3.335	8.065	21.593
P_{HF}	0.367	0.796	0.960	3.297	3.682
P_{LFn}	0.090	0.166	0.216	0.267	0.287
P_{LF}/P_{HF}	2.524	11.783	16.594	21.510	29.667

(a) Filling gaps with the reference method.

Metric	Missing beats [%]				
	5	10	15	20	25
P_{LF}	0.307	0.321	0.367	0.406	0.435
P_{HF}	0.172	0.398	0.430	0.558	0.415
P_{LFn}	0.053	0.080	0.084	0.157	0.116
P_{LF}/P_{HF}	3.419	2.959	4.404	5.299	6.363

(b) Filling gaps with the proposed method.

Table 4.4: Degradation of AR metrics (RMSE) when missing beats are randomly distributed. RMSE is normalized for P_{LF} and P_{HF}.

The performance difference of each interpolation method becomes very evident when fitting autoregressive models. In the case of this frequency

method, there is no doubt about the improvement that interpolating with the proposed method implies. Interpolation by the reference method causes a clear low-pass effect and significant distortion in the LF band. This is reflected both in a large error in P_{LF} and LF/HF ratio (Table 4.4), and visually in the spectra (Figure 4.7). Also, a frequency shift is observed for the HF and LF components, more evident in the reference method.

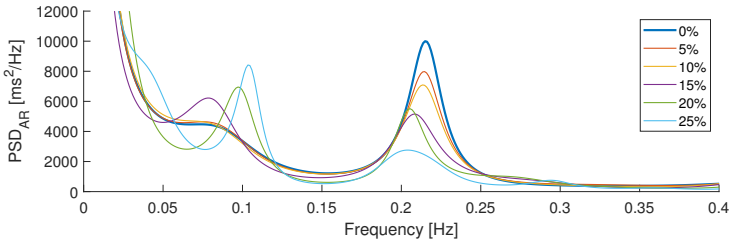

(a) Filling gaps with the reference method.

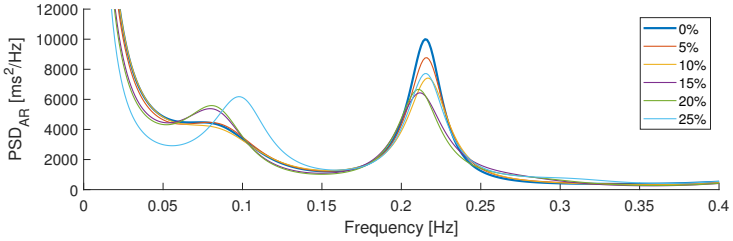

(b) Filling gaps with the proposed method.

Figure 4.7: AR spectral estimates from the same record with different loss rates randomly distributed.

Figure 4.8 shows the results of the Wilcoxon test for the proposed case. Only P_{HF} presents significant degradation from its reference values. Both P_{HF} and P_{LFn} can distinguish positions with 15% of missing pulses, while the LH/HF ratio can up to a 20%. P_{LF} cannot distinguish groups.

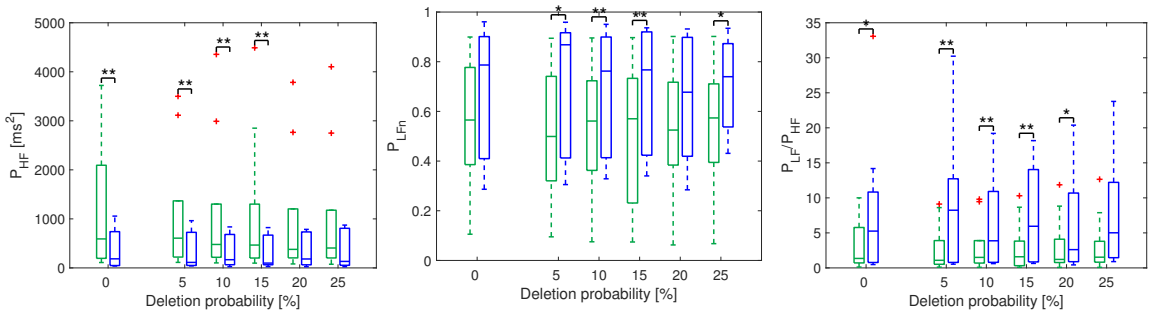

(a) P_{HF}. **(b)** P_{LFn}. **(c)** P_{LF}/P_{HF}.

Figure 4.8: ANS discrimination of AR metrics filling in the gaps with the proposed method when missed beats are randomly distributed. Green for supine, blue for tilt.

4.1.5 Poincaré plots

Metric	Missing beats [%]				
	5	10	15	20	25
SD1 [ms]	164.40	282.69	390.94	480.48	611.27
SD2 [ms]	148.19	255.89	344.54	422.61	557.75
SD12	0.553	0.604	0.637	0.644	0.646
S	19.34	50.16	86.31	121.03	199.42
Md [ms]	85.75	216.62	376.64	523.62	652.38
Sd [ms]	208.59	311.66	349.86	351.33	493.32

(a) Without preprocessing.

Metric	Missing beats [%]				
	5	10	15	20	25
SD1 [ms]	0.971	1.794	2.355	2.991	3.076
SD2 [ms]	4.046	5.322	6.547	8.799	8.272
SD12	0.028	0.038	0.041	0.067	0.070
S	0.088	0.143	0.185	0.193	0.156
Md [ms]	2.595	3.879	5.357	6.185	5.833
Sd [ms]	3.515	4.125	4.504	6.153	5.950

(b) Removing outliers.

Metric	Missing beats [%]				
	5	10	15	20	25
SD1 [ms]	3.900	4.911	13.937	18.646	26.884
SD2 [ms]	3.040	4.303	107.949	113.667	116.166
SD12	0.035	0.052	0.136	0.154	0.154
S	0.198	0.225	2.839	4.120	6.847
Md [ms]	2.859	4.093	61.620	60.181	54.089
Sd [ms]	4.006	4.242	95.273	105.444	113.524

(c) Filling gaps with the reference method.

Metric	Missing beats [%]				
	5	10	15	20	25
SD1 [ms]	1.277	1.593	1.476	3.923	3.952
SD2 [ms]	0.698	2.110	2.928	4.633	6.816
SD12	0.011	0.023	0.024	0.051	0.049
S	0.070	0.082	0.086	0.199	0.194
Md [ms]	0.773	1.858	2.961	3.762	4.888
Sd [ms]	0.926	1.413	1.371	3.774	6.680

(d) Filling gaps with the proposed method.

Table 4.5: Degradation of Poincaré metrics (RMSE) when missing beats are randomly distributed. RMSE is normalized for S

As with time-domain metrics, using Poincaré plots without preprocessing causes a large error in all the metrics. Removing outliers from the R-R series without interpolation produces the best results along with interpolating using the proposed method. However, the results of the Wilcoxon test indicate significant degradations from their reference values for SD2, S and Md using the proposed method. This, added to the higher cost and complexity of the method, makes the case removing outliers more recommendable. Errors are in the order of milliseconds, so it can be considered that there is almost no degradation in the metrics.

SD1, SD12 and S are the only metrics that achieve a supine-tilt differentiation removing outliers (Figure 4.9). In addition, the combination of SD1 and SD2 in SD12 separates more clearly the distributions belonging to the supine and tilt groups. All three metrics include the information from SD1, related to rapid pulse-to-pulse variations.

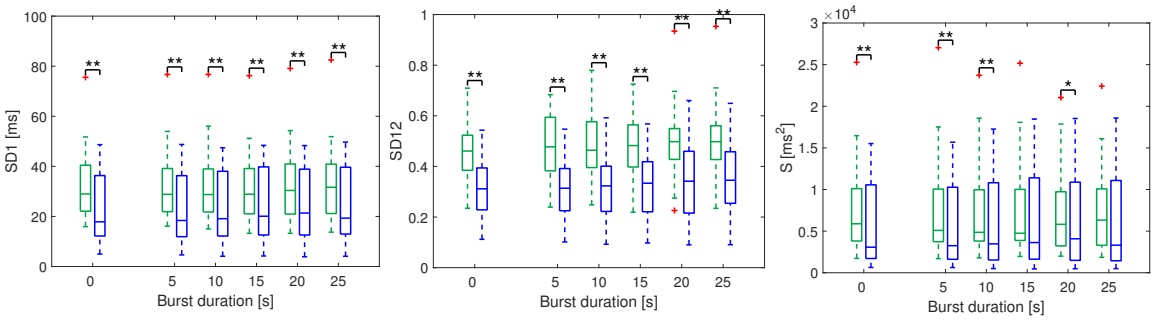

(a) SD1. **(b)** SD12. **(c)** S.

Figure 4.9: ANS discrimination of Poincaré metrics removing outliers when missed beats are randomly distributed. Green for supine, blue for tilt.

4.1.6 Symbolic metrics

Metric	Missing beats [%]				
	5	10	15	20	25
PIP [%]	3.781	7.489	11.010	15.318	16.953
IALS [beats^{-1}]	0.039	0.0758	0.110	0.154	0.171
PSS [%]	9.952	17.819	23.618	28.915	29.968
PAS [%]	6.402	12.891	18.164	25.512	25.224

(a) Without preprocessing.

Metric	Missing beats [%]				
	5	10	15	20	25
PIP [%]	3.077	5.189	8.559	11.371	13.761
IALS [beats^{-1}]	0.029	0.053	0.089	0.117	0.140
PSS [%]	3.964	8.024	13.347	18.095	23.275
PAS [%]	3.698	6.998	8.773	10.207	12.962

(b) Filling gaps with the reference method.

Metric	Missing beats [%]				
	5	10	15	20	25
PIP [%]	1.585	2.335	3.960	5.185	5.513
IALS [beats^{-1}]	0.017	0.029	0.044	0.064	0.084
PSS [%]	3.718	7.170	10.675	15.174	19.513
PAS [%]	3.654	5.699	6.862	9.587	11.920

(c) Filling gaps with the proposed method.

Table 4.6: Degradation of symbolic metrics (RMSE) when missing beats are randomly distributed.

Symbolic metrics have a particular response to detection losses. Just as in other methods it is necessary to eliminate the outliers of the series or fill in the gaps with some precision, in symbolic methods it is only important to obtain the actual direction of the acceleration between each pulse. Perfect results could be achieved with a series with absurd values from the physiological point of view simply by making the series increase or decrease in the appropriate instants. Therefore, it is possible that the preprocessing techniques used in the previous methods are not the most appropriate.

In view of the results (Table 4.6), it seems that the most indicated for randomly distributed missed pulses is the proposed method, whose results in the Wilcoxon test are shown in Figure 4.10.

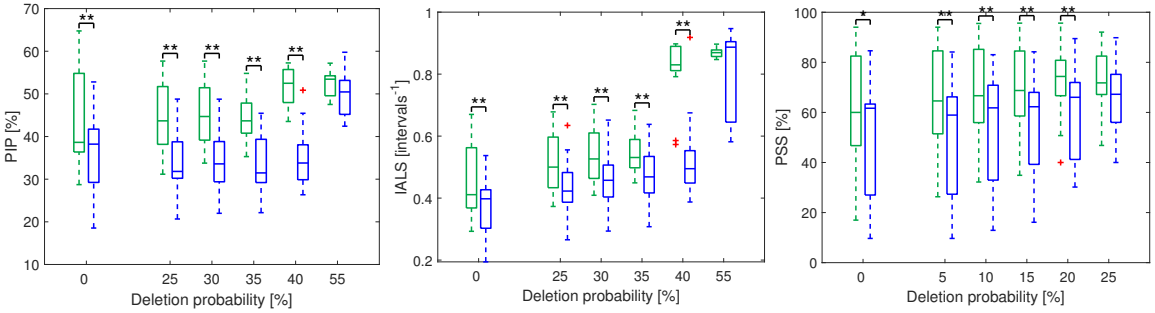

(a) PIP. **(b)** IALS. **(c)** PSS.

Figure 4.10: ANS discrimination of symbolic metrics filling in the gaps with the proposed method when missed beats are randomly distributed. Green for supine, blue for tilt.

This method achieves an excellent robustness of PIP, which has no significant variations from its reference values. The rest of the metrics do have them (IALS and PSS starting at 5% and PAS at 10% of missed beats), although they remain robust to discriminate the states of the ANS. Both PIP, IALS and PSS are higher in the supine case, which means that there is a higher

fragmentation. This is consistent to the higher HF modulation produced by a parasympathetic predominance. The only metric that does not manage to differentiate states is PAS. This probably occurs because it is a measure of very extreme fragmentation, which occurs only in pathological cases, as in coronary artery disease [32], rather than in mere increased sympathetic activity situations.

4.2 Bursts of missed beats

4.2.1 Time-domain metrics

Metric	Burst duration [s]					
	10	20	30	40	50	60
MHR [bpm]	0.61	0.78	0.96	1.30	1.54	1.91
SDNN [s]	1.02	2.03	3.15	4.43	5.91	7.66
SDSD [s]	1.49	2.93	4.54	6.38	8.51	11.05
RMSSD [s]	1.49	2.92	4.52	6.34	8.45	10.96
pNN50 [%]	2.05	2.65	3.48	4.64	4.90	4.61

(a) Without preprocessing.

Metric	Burst duration [s]					
	10	20	30	40	50	60
MHR [bpm]	0.10	0.45	0.62	0.90	1.09	1.31
SDNN [ms]	2.24	3.64	4.37	4.64	6.53	8.37
SDSD [ms]	2.06	3.09	3.71	4.57	5.13	5.76
RMSSD [ms]	2.05	3.07	3.70	4.55	5.11	5.73
pNN50 [%]	1.56	2.31	3.03	4.29	4.68	4.29

(b) Removing outliers.

Metric	Burst duration [s]					
	10	20	30	40	50	60
MHR [bpm]	0.28	0.52	0.82	1.54	1.52	2.21
SDNN [ms]	3.96	6.38	8.10	9.39	14.14	13.81
SDSD [ms]	7.05	8.87	10.35	12.54	15.27	17.51
RMSSD [ms]	7.02	8.83	10.31	12.49	15.20	17.43
pNN50 [%]	3.85	6.37	8.28	10.73	12.78	14.60

(c) Filling gaps with the reference method.

Metric	Burst duration [s]					
	10	20	30	40	50	60
MHR [bpm]	0.96	1.80	2.72	3.86	4.88	6.30
SDNN [ms]	15.65	24.42	30.98	38.01	42.17	43.59
SDSD [ms]	4.83	5.56	5.98	6.79	8.23	8.48
RMSSD [ms]	4.80	5.54	5.96	6.76	8.20	8.46
pNN50 [%]	2.60	4.38	6.26	8.64	10.54	12.19

(d) Filling gaps with the proposed method.

Table 4.7: Degradation of time-domain metrics (RMSE) when missing beats are distributed in bursts.

In this case there is no question about performing preprocessing, as there is only one prominent peak to be eliminated in the R-R series. Leaving this peak causes the degradation of SDNN, SDSD and RMSSD to increase proportionally to the size of the burst, producing huge errors (Table 4.7a). Note that in this case units are seconds instead of milliseconds. MHR and pNN50 are much less affected, and the degradation is mainly due to the lack of information provided

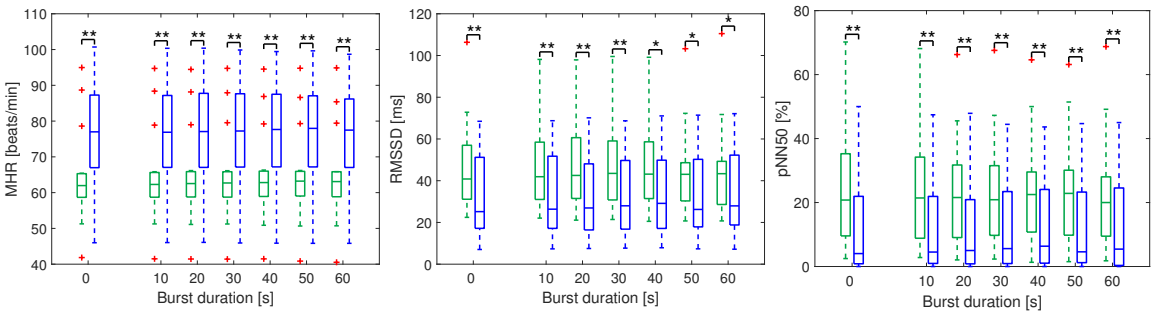

(a) MHR. **(b)** RMSSD. **(c)** pNN50.

Figure 4.11: ANS discrimination of time-domain metrics removing outliers (without interpolation) when missed pulses are distributed in bursts. Green for supine, blue for tilt.

by the missing pulses. The interpolation methods do not improve the results in this case either, as expected, since the correction of such large gaps is less accurate as the reference pulses are lost (Tables 4.7c and 4.7d). Even for 5-second bursts, better results are obtained without interpolation. Time-domain methods do not depend as much on the size of the burst as on the number of samples remaining and their representativeness of the whole series. For the two-minute series discussed in this work, it can be seen from Table 4.7b and Figure 4.11 that the results are hardly affected even by 60-second bursts, which represent half of the sample, merely removing the peak from the R-R series. There is no significant degradation for any metric from their reference values. These results indicate that time-domain methods are robust against both types of errors with simple preprocessing eliminating outliers.

4.2.2 Welch's method

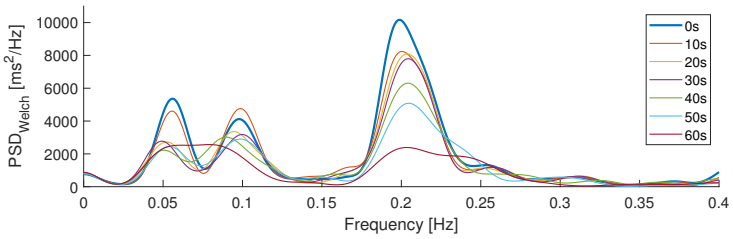

(a) Detecting gaps.

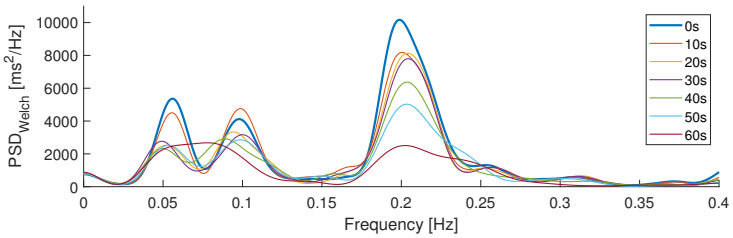

(b) Filling gaps with the reference method.

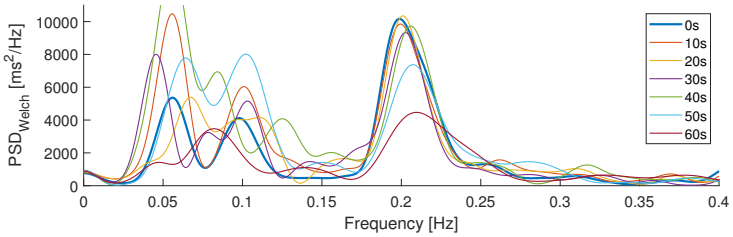

(c) Filling gaps with the proposed method.

Figure 4.12: Welch's spectral estimates from the same record with different burst durations.

In the case of bursts the differences between methods are not so clear. In Figure 4.12, it can be seen how the reference method obtains almost identical spectra to the case detecting gaps. The higher degradation of the LF band in the proposed case is not consistent in the other examples. This can be seen in Table 4.8c, where the LF error is even slightly lower than in the other two

Metric	Burst duration [s]					
	10	20	30	40	50	60
P_{LF}	0.371	0.513	0.588	0.722	0.888	1.021
P_{HF}	0.599	0.754	0.789	0.933	1.028	1.140
P_{LFn}	0.062	0.080	0.073	0.095	0.108	0.133
P_{LF}/P_{HF}	0.830	1.205	1.252	1.509	1.812	2.718

(a) Detecting gaps.

Metric	Burst duration [s]					
	10	20	30	40	50	60
P_{LF}	0.306	0.478	0.581	0.706	0.865	1.016
P_{HF}	0.620	0.747	0.790	0.943	1.032	1.150
P_{LFn}	0.066	0.084	0.076	0.095	0.110	0.138
P_{LF}/P_{HF}	0.870	1.253	1.249	1.528	1.885	3.207

(b) Filling gaps with the reference method.

Metric	Burst duration [s]					
	10	20	30	40	50	60
P_{LF}	0.342	0.374	0.482	0.623	0.711	0.823
P_{HF}	0.452	0.537	0.613	0.719	0.743	0.807
P_{LFn}	0.098	0.091	0.090	0.135	0.158	0.144
P_{LF}/P_{HF}	2.193	2.426	1.953	2.498	2.985	2.723

(c) Filling gaps with the proposed method.

Table 4.8: Degradation of Welch's metrics (RMSE) when missing beats are distributed in bursts. RMSE is normalized for P_{LF} and P_{HF}.

methods. The proposed method achieves non-significant differences for all the metrics from their reference values while the other two present differences in P_{LF} and P_{HF}. P_{HF} is the only robust metric in all cases for ANS discrimination (Figure 4.13).

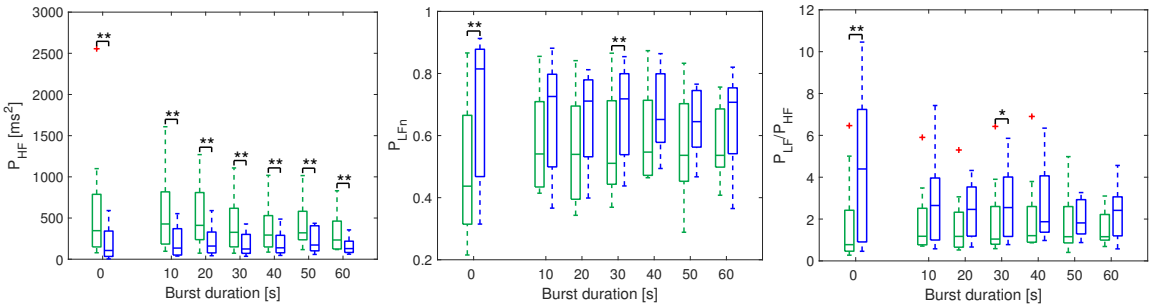

(a) P_{HF}. **(b)** P_{LFn}. **(c)** P_{LF}/P_{HF}.

Figure 4.13: ANS discrimination of Welch's metrics filling in the gaps with the proposed method when missed beats are distributed in bursts. Green for supine, blue for tilt.

4.2.3 Averaged Lomb's method

The behavior of this method in presence of bursts is particular. In the case without filling gaps, the error increases as the window grows until it reaches the 60-second burst, where it falls suddenly. This is due to the periodogram averaging. For samples like those in this work of 120 seconds, 3 periodograms are averaged for each recording using 60-second windows with 30-second overlap (from 0 to 60 , from 30 to 90 and from 60 to 120 seconds). In the Welch's method, the central window is always complete thanks to the interpolation of the R-R series using the IPFM model. However, in the case of Lomb removing outliers, the central window has fewer samples as the duration of the burst increases, producing the oscillation shown in Figure 4.14 (note that the oscillation reaches its maximum with the burst of 50 seconds instead of 60 seconds). When the 60-second burst is reached, the center window has no

samples and therefore no spectrum is calculated. Averaging is done with the other two windows. This makes the variance of the estimate greater than the case without the burst, because averaging is done with two windows instead of three, but the error is less than with three windows with missing samples.

Metric	Burst duration [s]					
	10	20	30	40	50	60
P_{LF}	0.198	0.366	0.661	1.038	1.569	0.546
P_{HF}	0.318	0.521	0.892	1.692	4.026	0.534
P_{LFn}	0.049	0.062	0.072	0.109	0.214	0.113
P_{LF}/P_{HF}	1.099	1.131	1.185	2.396	3.744	2.260

(a) Removing outliers.

Metric	Burst duration [s]					
	10	20	30	40	50	60
P_{LF}	0.229	0.391	0.519	0.587	0.847	0.836
P_{HF}	0.528	0.669	0.713	0.876	0.993	1.057
P_{LFn}	0.063	0.076	0.073	0.100	0.104	0.127
P_{LF}/P_{HF}	0.926	1.287	1.384	1.710	2.030	3.435

(b) Filling gaps with the reference method.

Metric	Burst duration [s]					
	10	20	30	40	50	60
P_{LF}	0.474	0.415	0.530	0.801	0.792	0.578
P_{HF}	0.400	0.428	0.447	0.621	0.632	0.749
P_{LFn}	0.103	0.089	0.105	0.147	0.140	0.129
P_{LF}/P_{HF}	1.755	2.142	1.949	2.751	2.636	2.160

(c) Filling gaps with the proposed method.

Table 4.9: Degradation of Lomb's metrics (RMSE) when missing beats are distributed in bursts. RMSE is normalized for P_{LF} and P_{HF}.

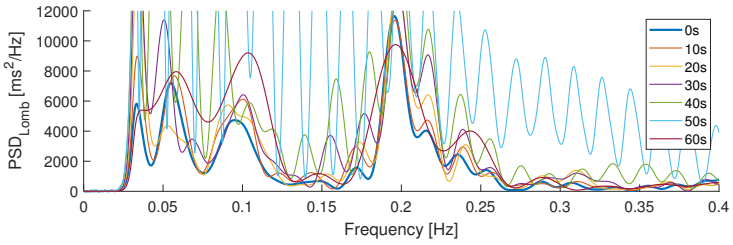

(a) Removing outliers.

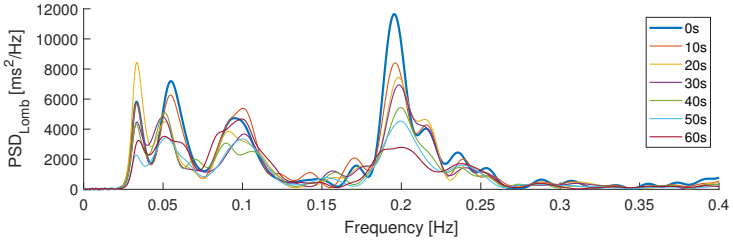

(b) Filling gaps with the reference method.

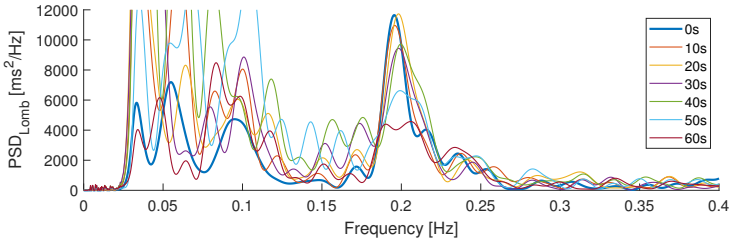

(c) Filling gaps with the proposed method.

Figure 4.14: Lomb's spectral estimates from the same record with different burst durations.

To better understand the burst effect, results have been recalculated using 120-second periodograms without averaging (Table 4.10). These results show

lower degradation even for 10-second bursts. This is due to the strong degradation of the periodogram calculated with the central window where the burst is located. The conclusion to be drawn is that degradation becomes very important when the burst duration is of the same order as the periodogram window.

Metric	Burst duration [s]					
	10	20	30	40	50	60
P_{LF}	0.230	0.414	0.674	0.982	1.391	2.148
P_{HF}	0.259	0.415	0.607	0.886	1.159	1.709
P_{LFn}	0.041	0.045	0.046	0.067	0.081	0.099
P_{LF}/P_{HF}	0.974	0.919	1.002	1.698	1.942	1.909

(a) Removing outliers.

Metric	Burst duration [s]					
	10	20	30	40	50	60
P_{LF}	0.194	0.312	0.404	0.476	0.639	0.610
P_{HF}	0.457	0.558	0.586	0.712	0.801	0.873
P_{LFn}	0.058	0.063	0.061	0.081	0.089	0.110
P_{LF}/P_{HF}	0.929	1.187	1.356	1.668	2.244	3.174

(b) Filling gaps with the reference method.

Metric	Burst duration [s]					
	10	20	30	40	50	60
P_{LF}	0.238	0.227	0.362	0.446	0.517	0.436
P_{HF}	0.287	0.330	0.337	0.457	0.467	0.498
P_{LFn}	0.066	0.060	0.078	0.102	0.113	0.106
P_{LF}/P_{HF}	1.581	2.110	1.387	2.257	2.449	1.886

(c) Filling gaps with the proposed method.

Table 4.10: Degradation of Lomb's metrics (RMSE) when missing beats are distributed in bursts. RMSE is normalized for P_{LF} and P_{HF}. Using 120-second periodograms.

In this case, the proposed method is the best way to maintain controlled degradation. Both P_{LFn} and LH/HF ratio have a non-significant degradation from their reference values with up to 60-second bursts. P_{HF} is the best metric to discriminate between tilt test positions, achieving significant differences with bursts of up to 60 seconds (Figure 4.15). P_{LF} cannot distinguish supine and tilt groups.

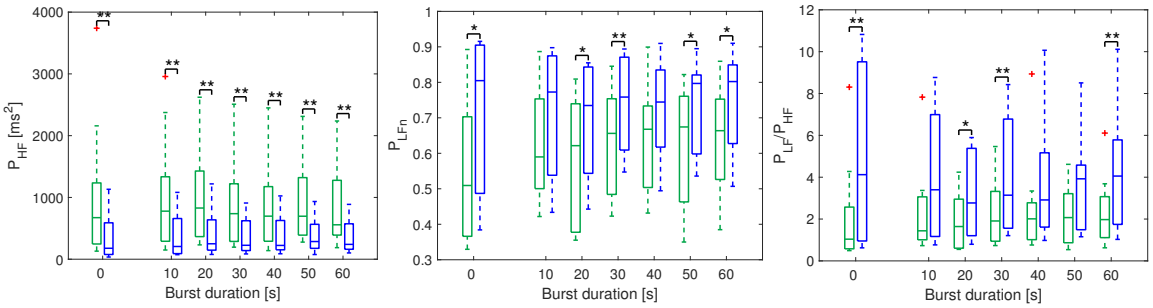

(a) P_{HF}. **(b)** P_{LFn}. **(c)** P_{LF}/P_{HF}.

Figure 4.15: ANS discrimination of Lomb's metrics filling in the gaps with the proposed method when missed beats are distributed in burst. Using 120-second periodograms. Green for supine, blue for tilt.

4.2.4 AR model

Both methods have strong degradations in the LF/HF ratio from its reference values, less in the proposed method case. Figure 4.16 shows a degradation example for each method. A shift in the HF component central frequency is observed as for randomly distributed missed beats, higher in the proposed

Metric	Burst duration [s]					
	10	20	30	40	50	60
P_{LF}	0.380	0.424	0.544	0.546	0.482	0.712
P_{HF}	0.753	0.679	0.835	0.748	0.797	0.900
P_{LFn}	0.167	0.147	0.183	0.125	0.145	0.171
P_{LF}/P_{HF}	10.492	9.505	9.863	3.336	4.701	5.515

(a) Filling gaps with the reference method.

Metric	Burst duration [s]					
	10	20	30	40	50	60
P_{LF}	0.581	0.416	0.556	0.602	0.644	0.833
P_{HF}	0.397	0.563	0.686	0.706	0.657	0.872
P_{LFn}	0.141	0.147	0.169	0.172	0.193	0.232
P_{LF}/P_{HF}	5.671	5.628	5.371	6.843	7.666	5.533

(b) Filling gaps with the proposed method.

Table 4.11: Degradation of AR metrics (RMSE) when missing beats are distributed in bursts. RMSE is normalized for P_{LF} and P_{HF}.

method. The Wilcoxon test shows this method achieve non-significant differences in more cases: only P_{HF} presents significant degradation from its reference values starting at 30-second bursts. However, is the only metric capable of distinguish positions in presence of bursts (Figure 4.17).

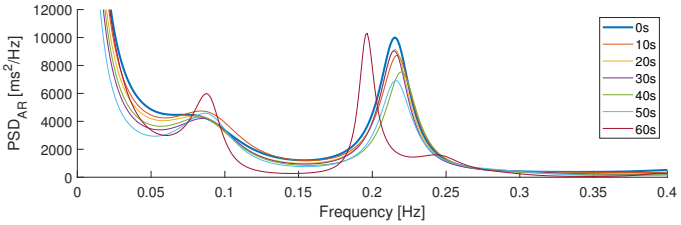

(a) Filling gaps with the reference method.

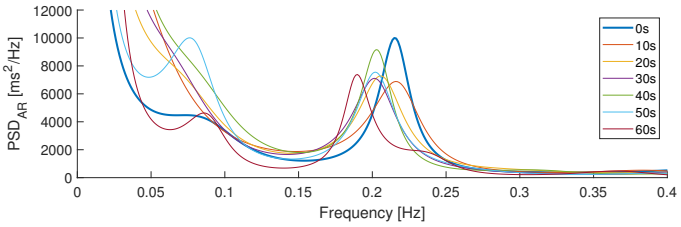

(b) Filling gaps with the proposed method.

Figure 4.16: AR spectral estimates from the same record with different burst durations.

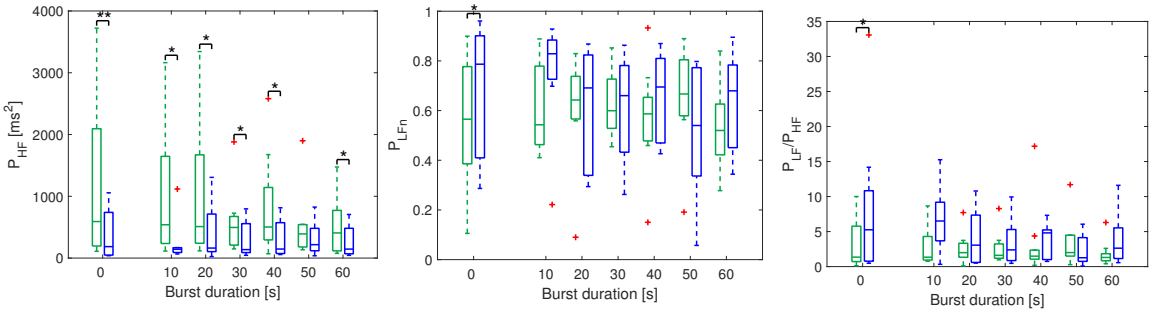

(a) P_{HF}. **(b)** P_{LFn}. **(c)** P_{LF}/P_{HF}.

Figure 4.17: ANS discrimination of AR metrics filling in the gaps with the proposed method when missed beats are distributed in bursts. Green for supine, blue for tilt.

4.2.5 Poincaré plots

The large outlier in the R-R series produces errors several orders of magnitude higher than the metrics (Table 4.12, units are in seconds in the case without

Metric	Burst duration [s]					
	10	20	30	40	50	60
SD1 [s]	1.059	2.076	3.213	4.515	6.023	7.817
SD2 [s]	1.008	2.014	3.136	4.419	5.891	7.641
SD12	0.637	0.639	0.640	0.641	0.644	0.645
S	536.6	1983.8	4693.0	9163.3	$16x10^3$	$27x10^3$
Md [s]	0.287	0.635	1.068	1.616	2.330	3.28
Sd [s]	1.451	2.837	4.375	6.120	8.105	10.428

(a) Without preprocessing.

Metric	Burst duration [s]					
	10	20	30	40	50	60
SD1 [ms]	1.462	2.185	2.626	3.236	3.628	4.078
SD2 [ms]	3.309	5.122	6.092	6.312	8.886	11.667
SD12	0.020	0.024	0.029	0.032	0.032	0.040
S	0.086	0.121	0.157	0.177	0.257	0.344
Md [ms]	2.855	4.309	5.212	5.701	8.054	10.297
Sd [ms]	2.392	4.186	4.794	5.238	6.256	7.999

(b) Removing outliers.

Metric	Burst duration [s]					
	10	20	30	40	50	60
SD1 [ms]	4.987	6.273	7.321	8.873	10.799	12.382
SD2 [ms]	4.516	7.435	9.729	11.823	17.491	17.074
SD12	0.048	0.055	0.059	0.084	0.075	0.103
S	0.242	0.332	0.395	0.441	0.614	0.614
Md [ms]	5.114	7.975	11.716	13.738	22.196	20.932
Sd [ms]	4.642	5.790	6.569	6.663	7.883	8.848

(c) Filling gaps with the reference method.

Metric	Burst duration [s]					
	10	20	30	40	50	60
SD1 [ms]	3.417	3.934	4.231	4.803	5.823	6.003
SD2 [ms]	23.271	36.353	46.395	56.911	62.725	64.878
SD12	0.105	0.142	0.175	0.202	0.209	0.221
S	0.456	0.555	0.691	0.776	0.914	0.817
Md [ms]	14.373	26.528	39.030	52.382	62.149	65.832
Sd [ms]	18.586	23.717	22.584	20.006	14.157	12.837

(d) Filling gaps with the proposed method.

Table 4.12: Degradation of Poincaré metrics (RMSE) when missing beats are distributed in bursts. RMSE is normalized for S.

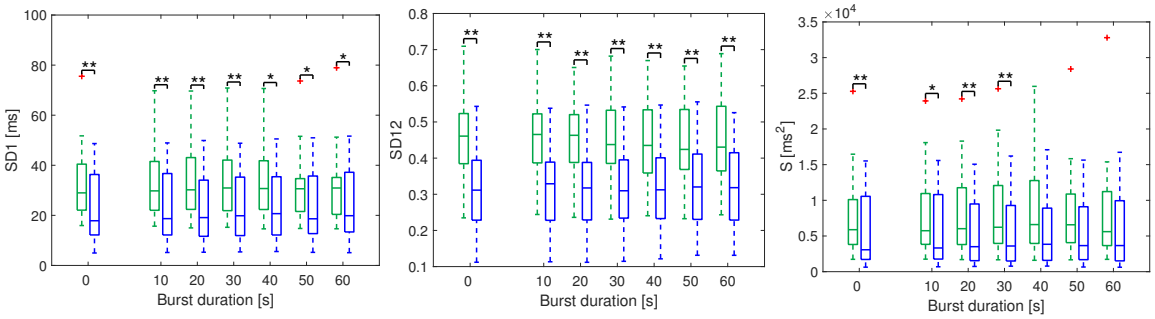

(a) SD1. **(b)** SD12. **(c)** S.

Figure 4.18: ANS discrimination of Poincaré metrics removing outliers when missed beats are distributed in bursts. Green for supine, blue for tilt.

preprocessing). In this case the error does increase in all metrics. Among the preprocessing methods tested, the one that obtains the best results is to eliminate the peak without interpolation. No metric suffers significant degradation from its reference values even for 60-second bursts. Figure 4.18 shows the results of the Wilcoxon test for this case. Both SD1 and SD12 are capable of distinguish positions for any burst duration. Again, greater differences are achieved by SD12, with p-values below 0.025 in all cases. It is therefore the most recommended metric in this task both with randomly distributed errors and in bursts. S is also capable of distinguishing positions with up to 30-second bursts.

4.2.6 Symbolic metrics

In the case of bursts, the option without preprocessing is the best one (Table 4.13). Filling in the gaps introduces pulses without fragmentation using either methods. Thus, the metrics suffer a strong degradation as fragmentation represents a lower percentage of the total pulses. Without preprocessing, degradation from its reference values is not significant except in the IALS case.

Metric	Burst duration [s]					
	10	20	30	40	50	60
PIP [%]	1.348	1.978	2.193	2.731	3.058	3.764
IALS [beats^{-1}]	0.014	0.021	0.023	0.029	0.035	0.046
PSS [%]	3.501	5.020	5.670	6.389	7.225	9.830
PAS [%]	2.819	4.617	4.045	4.856	7.288	6.588

(a) Without preprocessing.

Metric	Burst duration [s]					
	10	20	30	40	50	60
PIP [%]	4.523	7.649	11.237	14.871	18.462	21.377
IALS [beats^{-1}]	0.048	0.080	0.119	0.157	0.193	0.225
PSS [%]	3.234	4.851	5.088	6.331	5.903	7.002
PAS [%]	4.141	5.181	7.109	8.477	9.055	10.404

(b) Filling gaps with the reference method.

Metric	Burst duration [s]					
	10	20	30	40	50	60
PIP [%]	2.783	4.445	5.901	7.374	8.763	10.780
IALS [beats^{-1}]	0.034	0.060	0.094	0.122	0.164	0.198
PSS [%]	8.476	14.809	19.471	23.520	28.321	30.903
PAS [%]	5.672	8.905	12.205	14.488	18.880	22.976

(c) Filling gaps with the proposed method.

Table 4.13: Degradation of symbolic metrics (RMSE) when missing beats are distributed in bursts.

PIP and IALS are the best metrics to distinguish supine and tilt groups, with up to 60 second bursts (Figure 4.19).

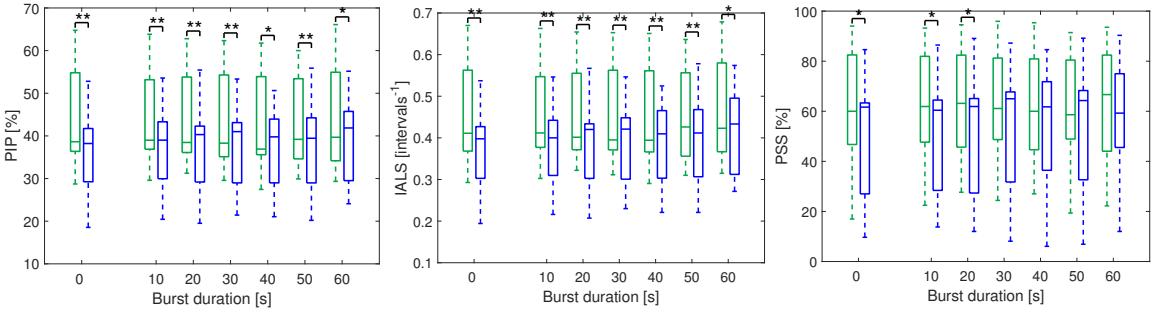

(a) PIP. **(b)** IALS. **(c)** PSS.

Figure 4.19: ANS discrimination of symbolic metrics without preprocessing when missed beats are randomly distributed. Green for supine, blue for tilt.

Chapter 5

Discussion

Before moving on to the conclusions, a number of issues need to be addressed. Firstly, time-domain metrics have demonstrated to be very robust and low cost. However, despite the good differentiation of the tilt-table test groups, these indexes are not very informative. For instance, an increase in MHR is related to a stress response (it should be understood that this refers to a persistent increase, not fluctuations over short periods, such as those that can be caused by sinus arrhythmia) and to a change in the sympathovagal balance. However, it is not possible to know by this measure alone whether there has been an increase in sympathetic tone, a parasympathetic withdrawal or both at the same time. In spite of their limitations, time-domain metrics may be a great approach for wearable applications for which no further information is needed and cost and power requirements are limited.

Frequency-domain metrics should be used for more information relating sympathetic and parasympathetic activity. For random distributed errors, filling gaps with the proposed method achieves the lowest degradation. However, this preprocessing implies an additional cost. For low percentages of missing beats (up to a 10%), the Lomb's method removing outliers is an excellent approach, achieving better results than Welch's detecting gaps. It is worth to remember that the latter performs a gap correction via the IPFM model. Filling the gaps at Lomb eliminates its main advantage and is not an improvement over filling them at Welch. AR models do not present any advantages in terms of cost-degradation relation. In the case of bursts, Lomb without filling in the gaps present a high degradation due to a total lack of signal and therefore is strongly recommended not to use. Also the AR models present a strong degradation. The frequency shift is probably due to a miscalculation of the sampling period from the R-R series, which is calculated as the mean interval. This shift may not be a problem in terms of power calculation. Although some methods manage to control degradation, the error with a 10-second burst is greater than for 25% random loss. The implementation of frequency methods should exclude bursts before spectral estimation. Even so, Lomb provides good results for 10-second bursts.

However, it presents the worst degradation with larger bursts.

Classical frequency analysis uses fixed bands where the different components are normally found: 0.04 to 0.15Hz for LF and 0.15 to 0.4Hz for HF. Recent studies have shown that respiratory information can be used to more accurately determine the limits of the HF component, obtaining more reliable metrics [34]. It has been considered that analysing these methods is beyond the scope of this thesis. In spite of the fact that the database has respiratory records, in a real case with wearables this signal must be derived from the same noisy signal where the pulses are detected. This implies a double degradation: that of the spectrum and that of the window. A separate study must therefore be made of the degradation of the respiratory estimate derived from the photoplethysmogram, to which must be added the spectrum degradation seen in this work. Frequency metrics are expensive in terms of computing, which would limit their application in some wearables.

Poincaré plots behave similarly to temporal metrics. Eliminating outliers is both necessary and sufficient to obtain robust results both for random distributions and bursts. SD1 related metrics are the only ones able to differentiate supine and tilt groups, being SD12 especially robust. It is often suggested that Poincaré metrics are able to measure qualities of the variability that are nonlinear and independent of the standard linear methods. This is rejected in [35], as SD1 and SD2 are related to the autocovariance function and standard time-domain measures like SDSD and SDRR ($SDRR = \frac{1}{\sqrt{2}}\sqrt{SD1^2 + SD2^2}$). Several authors modified the chart by using a time lag of more than one beat to get more informative parameters, since a heart beat influences not only the beat immediately following it, but also 6 to 10 beats downstream, possibly as a consequence of respiratory sinus arrhythmia [30]. When a lag is included, the plot takes the name of lagged Poincaré plot. Although lagged Poincaré plots can achieve the desired HRV non-linear metrics, they are difficult to relate to physiological processes. For this reason, no lag is included in this work.

Although symbolic metrics present strong degradations in the random case, they are robust in distinguishing tilt and supine groups. Filling in the gaps with the proposed method improves the robustness. In the case of bursts, degradation is lower and it is preferable not to preprocess. In [32], fragmentation indices outperformed standard time and frequency-domain measures in separating subjects from patients with coronary artery disease. The authors argue that in pathological cases, such as this disease, changes in the direction of acceleration are more frequent, *i.e.*, there is more fragmentation. In addition, these metrics have some advantages, among which are: they are easy to implement, are independent of the mean heart rate and the amplitude of the time series, are less affected by nonstationarities and are robust against ectopic beats. Removing outliers caused by missed data is not as simple as it is in time-domain metrics. The treatment of the gaps is not trivial and can be

counterproductive, as the peaks may have the right acceleration. Despite being designed to find impairments of the autonomic nervous system, they have been proven to be also effective in distinguishing between physiological states such as those of the tilt-table test.

In view of these results, choosing a method depends largely on the application. It has been seen that the frequency methods are very informative, but they imply an additional cost. Thus, for devices that require less processing, time, symbolic and Poincaré parameters are a cheap and robust option simply by eliminating outliers. However, the information they provide greatly limits their scope of application. In devices with higher processing capacity, or in those that perform processing outside the device, frequency methods will provide additional information.

It must be remembered that the aim of this work is not to obtain a single, general solution that works best in noisy environments. The objective is to analyse different methods, commonly used and currently being studied as non-invasive techniques for assessing the autonomic nervous system, in order to study the different effects caused by missing data and set the limits where measures are not longer reliable. This aims to provide a general idea of the problems that may arise in each case and possible improvements in the preprocessing phase. For each metric it should be assessed what improvements it produces and what its limitations are.

The same happens to the application of these metrics. Besides degradations, the ability to distinguish two specific groups in a controlled environment (supine and tilt) has been tested. The metrics that have achieved the best results in this task do not have to be the same when, for example, trying to separate groups according to whether or not they have a disease. Therefore, once the overview provided by this work is obtained, each technique should be investigated in the context of a specific application. Moreover, it is expected for tilt-table test to provoke a significant change in the ANS. Other contexts can lead to more subtle changes, where some successful methods may fail.

One of the limitations of this work for direct application in the wearables market is the use of an electrocardiographic signal as reference. Normally, these devices use photoplethysmography instead. Thus, they do not measure the pulse directly on the heart, but on the periphery. This makes the results not completely transferable to the practical case. Nevertheless, they can be a good approximation since it has been proven that pulse rate variability obtained from this signal is a good substitute for heart rate variability obtained from the ECG [36]. Intuitively, degradations can be assumed to be the same, since the detection series are distinguished only by small variations and degradations are first and foremost method-related.

Finally, this work is focused on observing the deterioration of HRV metrics with missing data. The proposed methods are also capable of dealing with pulses introduced by false positives, however, they have not been tested in this

context. For example, in the case of device movement, it has been assumed that the noise level causes no pulses to be detected for a few seconds (bursts). Nonetheless, false detections in this segment may be mistaken for real pulses. This is one of the worst possible scenarios, since losing the reference makes it impossible to distinguish actual pulses from incorrect ones. Solving this requires a previous stage of signal quality evaluation and/or detection of anomalies in the metrics at the end of the process. However, this is beyond the scope of this work.

Chapter 6

Conclusions and future lines

The main HRV methods have been reviewed and both their degradation and their ability to distinguish supine and tilt groups have been evaluated. A novel approach for filling in the gaps has been proposed, obtaining better results than the reference method. In addition, a simulation protocol for missing data environments has been presented. Detecting outliers caused by missing data is a common task to improve the robustness of all metrics. However, its further treatment varies between methods:

- Time-domain metrics: the outliers from the R-R series cause large errors if not processed. Removing outliers without filling them proves to be the best option both for randomly distributed missed beats and bursts.

- Welch's method: the proposed method improves the results for randomly distributed errors. Significant degradations occurs even for 10-second bursts. Discarding the window before averaging should be considered.

- Lomb's method: the proposed method improves the robustness for all the metrics when missed beats are randomly distributed. On the other hand, it is strongly recommended not to average periodograms in presence of bursts.

- AR model: the proposed method supposes a huge improvement against the reference method in the case of random distributed losses. Differences in the case of bursts are reduced, yet the proposed method is still recommended due to a lower degradation of the LF/HF ratio. A frequency shift is observed, especially in presence of bursts. This should be considered in applications such as respiratory rate estimation.

- Poincaré plots: it is strongly recommended to remove outliers before, although interpolation does not improve the results. Both for random distributions and bursts.

— Symbolic metrics: although large errors occur in all cases, the metrics are robust in terms of their ability to distinguish ANS states. The proposed method manages to maintain a more controlled degradation in the case of random losses. For the case of bursts it is best to eliminate outliers without interpolation.

As future lines, the methods must be tested in other databases, in order to validate results and extract common problems of each method, preferably recorded by wearables (although the ECG will also be required for validation). In addition, different preprocessing methods, different implementations of HRV methods and even other state-of-the-art metrics can be evaluated. Metrics have been evaluated against errors and their possible improvements. In order to use them in commercial devices, other parts of the process have to be investigated as well. Thus, a stage before pulse detection where the signal quality is evaluated will be very important to ensure a reference that can be trusted. Likewise, once the metrics are obtained, a postprocessing can be performed to discard those that are suspected to be wrong. Work should also be done on possible improvements to the proposed method, taking into account extreme cases that may not have appeared in this database. Finally, it should be noted that only an overview of each method has been given. For each specific application, a dedicated study should be made, since the different implementations may imply significant differences.

Chapter 7

Bibliography

[1] Leif Sörnmo and Pablo Laguna. *Bioelectrical signal processing in cardiac and neurological applications*, volume 8. Academic Press, 2005.

[2] A John Camm, Marek Malik, J Thomas Bigger, Günter Breithardt, Sergio Cerutti, RJ Cohen, Philippe Coumel, EL Fallen, HL Kennedy, RE Kleiger, et al. Heart rate variability: standards of measurement, physiological interpretation and clinical use. task force of the european society of cardiology and the north american society of pacing and electrophysiology. *European Heart Journal*, 17:354–381, 1996.

[3] Sheng Lu, He Zhao, Kihwan Ju, Kunson Shin, Myoungho Lee, Kirk Shelley, and Ki H Chon. Can photoplethysmography variability serve as an alternative approach to obtain heart rate variability information? *Journal of clinical monitoring and computing*, 22(1):23–29, 2008.

[4] Bruce M Koeppen and Bruce A Stanton. *Berne and levy physiology e-book*. Elsevier Health Sciences, 2017.

[5] Arthur C Guyton, John Edward Hall, et al. *Textbook of medical physiology*, volume 548. Saunders Philadelphia, 1986.

[6] Stephen Hales. *Statical essays*, volume 2. 1733.

[7] Sigmund Mayer. Studien zur physiologie des herzens und der blutgrfasse v. uber spntane blutdruck schwankungen. *Akad Wiss Wien Math Nat Kl*, 74:281–307, 1876.

[8] Gian Carlo Casolo, Piero Stroder, Claudia Signorini, Francesca Calzolari, Mauro Zucchini, Enrico Balli, Antonio Sulla, and Stefano Lazzerini. Heart rate variability during the acute phase of myocardial infarction. *Circulation*, 85(6):2073–2079, 1992.

[9] KE Sands, Marvin L Appel, Leonard S Lilly, Frederick J Schoen, Gilbert H Mudge Jr, and Richard J Cohen. Power spectrum analysis of heart rate

variability in human cardiac transplant recipients. *Circulation*, 79(1):76–82, 1989.

[10] Solange Akselrod, David Gordon, F Andrew Ubel, Daniel C Shannon, AC Berger, and Richard J Cohen. Power spectrum analysis of heart rate fluctuation: a quantitative probe of beat-to-beat cardiovascular control. *science*, 213(4504):220–222, 1981.

[11] Alberto Malliani, Massimo Pagani, Federico Lombardi, and Sergio Cerutti. Cardiovascular neural regulation explored in the frequency domain. *Circulation*, 84(2):482–492, 1991.

[12] Bruce Pomeranz, RJ Macaulay, Margaret A Caudill, Ilan Kutz, Dan Adam, David Gordon, Kenneth M Kilborn, A Clifford Barger, Daniel C Shannon, and Richard J Cohen. Assessment of autonomic function in humans by heart rate spectral analysis. *American Journal of Physiology-Heart and Circulatory Physiology*, 248(1):H151–H153, 1985.

[13] Massimo Pagani, Federico Lombardi, Stefano Guzzetti, Ornella Rimoldi, Raffaello Furlan, Paolo Pizzinelli, Giulia Sandrone, Gabriella Malfatto, Simonetta Dell'Orto, and Emanuela Piccaluga. Power spectral analysis of heart rate and arterial pressure variabilities as a marker of sympatho-vagal interaction in man and conscious dog. *Circulation research*, 59(2):178–193, 1986.

[14] BW Hyndman. The role of rhythms in homeostasis. *Kybernetik*, 15(4):227–236, 1974.

[15] U Rajendra Acharya, K Paul Joseph, Natarajan Kannathal, Choo Min Lim, and Jasjit S Suri. Heart rate variability: a review. *Medical and biological engineering and computing*, 44(12):1031–1051, 2006.

[16] Federico Lombardi, Giulia Sandrone, Silvia Pernpruner, Roberto Sala, Mario Garimoldi, Sergio Cerutti, Giuseppe Baselli, Massimo Pagani, and Alberto Malliani. Heart rate variability as an index of sympathovagal interaction after acute myocardial infarction. *The American journal of cardiology*, 60(16):1239–1245, 1987.

[17] Massimo Pagani, Gabriella Malfatto, Simona Pierini, Rodolfo Casati, Anna Maria Masu, Massimo Poli, Stefano Guzzetti, Federico Lombardi, Sergio Cerutti, and Alberto Malliani. Spectral analysis of heart rate variability in the assessment of autonomic diabetic neuropathy. *Journal of the autonomic nervous system*, 23(2):143–153, 1988.

[18] Stefano Guzzetti, Emanuela Piccaluga, Rodolfo Casati, Sergio Cerutti, Federico Lombardi, Massimo Pagani, and Alberto Malliani. Sympathetic predominance in essential hypertension: a study employing spectral

analysis of heart rate variability. *Journal of hypertension*, 6(9):711–717, 1988.

[19] J Hayward, G Chansin, and H Zervos. Wearable technology 2017-2027: Markets, players, forecasts. *IDTexEx Report*, 2017.

[20] David Hernando, Surya Roca, Jorge Sancho, Álvaro Alesanco, and Raquel Bailón. Validation of the apple watch for heart rate variability measurements during relax and mental stress in healthy subjects. *Sensors*, 18(8):2619, 2018.

[21] Elena Peralta, Jesus Lazaro, Raquel Bailon, Vaidotas Marozas, and Eduardo Gil. Optimal fiducial points for pulse rate variability analysis from forehead and finger photoplethysmographic signals. *Physiological measurement*, 40(2):025007, 2019.

[22] Eduardo Gil, Michele Orini, Raquel Bailón, José María Vergara, Luca Mainardi, and Pablo Laguna. Photoplethysmography pulse rate variability as a surrogate measurement of heart rate variability during non-stationary conditions. *Physiological measurement*, 31(9):1271, 2010.

[23] Nicola Montano, T Gnecchi Ruscone, Alberto Porta, Federico Lombardi, Massimo Pagani, and Alberto Malliani. Power spectrum analysis of heart rate variability to assess the changes in sympathovagal balance during graded orthostatic tilt. *Circulation*, 90(4):1826–1831, 1994.

[24] Juan Pablo Martínez, Rute Almeida, Salvador Olmos, Ana Paula Rocha, and Pablo Laguna. A wavelet-based ecg delineator: evaluation on standard databases. *IEEE Transactions on biomedical engineering*, 51(4):570–581, 2004.

[25] Javier Mateo and Pablo Laguna. Analysis of heart rate variability in the presence of ectopic beats using the heart timing signal. *IEEE Transactions on biomedical engineering*, 50(3):334–343, 2003.

[26] James McNames and Mateo Aboy. Reliability and accuracy of heart rate variability metrics versus ecg segment duration. *Medical and Biological Engineering and Computing*, 44(9):747–756, 2006.

[27] Elliott J Bayly. Spectral analysis of pulse frequency modulation in the nervous systems. *IEEE Transactions on Biomedical Engineering*, (4):257–265, 1968.

[28] Javier Mateo and Pablo Laguna. Improved heart rate variability signal analysis from the beat occurrence times according to the ipfm model. *IEEE Transactions on Biomedical Engineering*, 47(8):985–996, 2000.

[29] Pablo Laguna, George B Moody, and Roger G Mark. Power spectral density of unevenly sampled data by least-square analysis: performance and application to heart rate signals. *IEEE Transactions on Biomedical Engineering*, 45(6):698–715, 1998.

[30] Berik Koichubekov, Viktor Riklefs, Marina Sorokina, Ilya Korshukov, Lyudmila Turgunova, Yelena Laryushina, Riszhan Bakirova, Gulmira Muldaeva, Ernur Bekov, and Makhabbat Kultenova. Informative nature and nonlinearity of lagged poincaré plots indices in analysis of heart rate variability. *Entropy*, 19(10):523, 2017.

[31] Mimma Nardelli, Alberto Greco, Juan Bolea, Gaetano Valenza, Enzo Pasquale Scilingo, and Raquel Bailón. Reliability of lagged poincaré plot parameters in ultrashort heart rate variability series: Application on affective sounds. *IEEE journal of biomedical and health informatics*, 22(3):741–749, 2017.

[32] Madalena D Costa, Roger B Davis, and Ary L Goldberger. Heart rate fragmentation: a new approach to the analysis of cardiac interbeat interval dynamics. *Frontiers in physiology*, 8:255, 2017.

[33] Madalena D Costa, Roger B Davis, and Ary L Goldberger. Heart rate fragmentation: a symbolic dynamical approach. *Frontiers in physiology*, 8:827, 2017.

[34] Alberto Hernando, Jesús Lázaro, Eduardo Gil, Adriana Arza, Jorge Mario Garzón, Raúl López-Antón, Concepción de la Cámara, Pablo Laguna, Jordi Aguiló, and Raquel Bailón. Inclusion of respiratory frequency information in heart rate variability analysis for stress assessment. *IEEE journal of biomedical and health informatics*, 20(4):1016–1025, 2016.

[35] Michael Brennan, Marimuthu Palaniswami, and Peter Kamen. Do existing measures of poincare plot geometry reflect nonlinear features of heart rate variability? *IEEE transactions on biomedical engineering*, 48(11):1342–1347, 2001.

[36] Vala Jeyhani, Shadi Mahdiani, Mikko Peltokangas, and Antti Vehkaoja. Comparison of hrv parameters derived from photoplethysmography and electrocardiography signals. In *2015 37th Annual International Conference of the IEEE Engineering in Medicine and Biology Society (EMBC)*, pages 5952–5955. IEEE, 2015.

[37] David Hernando, Mimma Nardelli, Kyle Hocking, Jesús Lázaro, Bret Alvis, Eduardo Gil, Enzo P Scilingo, Daniel R Brophy, Gaetano Valenza, Pablo Laguna, et al. Effect of yoga on pulse rate variability measured from a venous pressure waveform. In *2019 41st Annual International Conference*

of the IEEE Engineering in Medicine and Biology Society (EMBC), pages 372–375. IEEE, 2019.

[38] Jesús Lázaro, Eduardo Gil, Raquel Bailón, Ana Mincholé, and Pablo Laguna. Deriving respiration from photoplethysmographic pulse width. *Medical & biological engineering & computing*, 51(1-2):233–242, 2013.

[39] R Almeida, E Pueyo, JP Martinez, AP Rocha, S Olmos, and P Laguna. A parametric model approach for quantification of short term qt variability uncorrelated with heart rate variability. In *Computers in Cardiology, 2003*, pages 165–168. IEEE, 2003.

[40] Christopher G Scully, Jinseok Lee, Joseph Meyer, Alexander M Gorbach, Domhnull Granquist-Fraser, Yitzhak Mendelson, and Ki H Chon. Physiological parameter monitoring from optical recordings with a mobile phone. *IEEE Transactions on Biomedical Engineering*, 59(2):303–306, 2011.

List of Abbreviations

ANS Autonomic Nervous System.

AV node Atrioventricular Node.

CNS Central Nervous System.

ECG Electrocardiography/Electrocardiogram.

HF High Frequency.

HR Heart Rate.

HRF Heart Rate Fragmentation.

HRV Heart Rate Variability.

LF Low Frequency.

MHR Mean Heart Rate.

PPG Photoplethysmogram.

PSD Power Spectral Density.

RMSE Root Mean Square Error.

RMSSD Root Mean Square of Successive Differences.

RSA Respiratory Sinus Arrhythmia.

SA node Sinoatrial Node.

SDNN Standard Deviation of the N-N interval.

SDSD Standard Deviation of Successive Differences.

SNR Signal to Noise Ratio.

VLF Very Low Frequency.

List of Figures

List of Tables